WL-TR-95-2116

# FUNDAMENTAL STUDIES IN CRYOGENIC COOLING OF POWER ELECTRONICS

L. C. CHOW    M. S. SEHMBEY
W. F. LU      C. J. CHUI
O. J. HAHN    M. R. PAIS

UNIVERSITY OF KENTUCKY
DEPARTMENT OF MECHANICAL ENGINEERING
LEXINGTON, KY 40506-0046
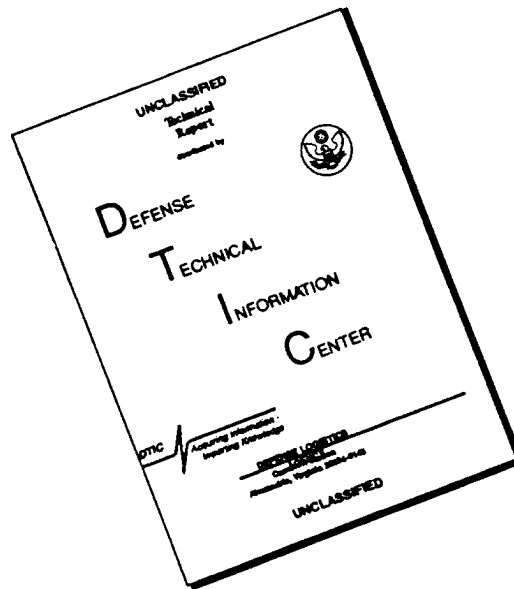
SEPTEMBER 1995

INTERIM REPORT FOR 09/01/94-08/31/95

APPROVED FOR PUBLIC RELEASE; DISTRIBUTION IS UNLIMITED.

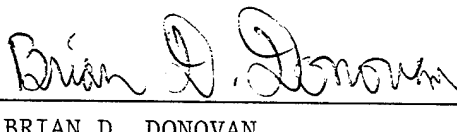DTIC QUALITY INSPECTED

1996061O 148

# DISCLAIMER NOTICE

THIS DOCUMENT IS BEST QUALITY AVAILABLE. THE COPY FURNISHED TO DTIC CONTAINED A SIGNIFICANT NUMBER OF PAGES WHICH DO NOT REPRODUCE LEGIBLY.
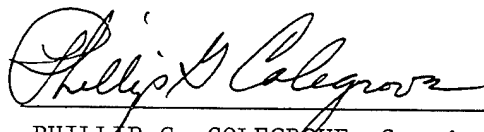
## NOTICE

When Government drawings, specifications, or other data are used for any purpose other than in connection with a definitely Government-related procurement, the United States Government incurs no responsibility or any obligation whatsoever. The fact that the government may have formulated or in any way supplied the said drawings, specifications, or other data, is not to be regarded by implication, or otherwise in any manner construed, as licensing the holder, or any other person or corporation; or as conveying any rights or permission to manufacture, use, or sell any patented invention that may in any way be related thereto.

This report is releasable to the National Technical Information Service (NTIS). At NTIS, it will be available to the general public, including foreign nations.

The technical report has been reviewed and is approved for publication.


BRIAN D. DONOVAN
Project Engineer
Electromechanical Technology Section

PHILLIP G. COLEGROVE, Section Chief
Electromechanical Technology Section
Power Technology Branch


MICHAEL D. BRAYDICH, LT COL, USAF
Chief, Aerospace Power Division
Aero Propulsion and Power Directorate

# REPORT DOCUMENTATION PAGE

Public reporting burden for this collection of information is estimated to average 1 hour per response, including the time for reviewing instructions, searching existing data sources, gathering and maintaining the data needed, and completing and reviewing the collection of information. Send comments regarding this burden estimate or any other aspect of this collection of information, including suggestions for reducing this burden, to Washington Headquarters Services, Directorate for Information Operations and Reports, 1215 Jefferson Davis Highway, Suite 1204, Arlington, VA 22202-4302, and to the Office of Management and Budget, Paperwork Reduction Project (0704-0188), Washington, DC 20503.

| 1. AGENCY USE ONLY (Leave blank) | 2. REPORT DATE SEP 1995 | 3. REPORT TYPE AND DATES COVERED INTERIM 09/01/94–08/31/95 |
|---|---|---|

**4. TITLE AND SUBTITLE**

Fundamental Studies in Cryogenic Cooling of Power Electronics

**5. FUNDING NUMBERS**

C F33615-91-C-2152
PE    63218
PR    1601
TA    05
WU    03

**6. AUTHOR(S)**

L. C. Chow        M. S. Sehmbey
W. F. Lu          C. J. Chui
O. J. Hahn        M. R. Pais

**7. PERFORMING ORGANIZATION NAME(S) AND ADDRESS(ES)**

University of Kentucky
Department of Mechanical Engineering
Lexington, KY  40506-0046

**8. PERFORMING ORGANIZATION REPORT NUMBER**

**9. SPONSORING/MONITORING AGENCY NAME(S) AND ADDRESS(ES)**

Aero Propulsion and Power Directorate
Wright Laboratory
Air Force Materiel Command
Wright Patterson AFB OH  45433-7650

**10. SPONSORING/MONITORING AGENCY REPORT NUMBER**

WL-TR-95-2116

**11. SUPPLEMENTARY NOTES**

**12a. DISTRIBUTION/AVAILABILITY STATEMENT**

Approved for public release; Distribution is unlimited.

**12b. DISTRIBUTION CODE**

**13. ABSTRACT (Maximum 200 words)**

This report is divided into three different studies. The first study deals with the critical heat flux in spray cooling. A new correlation is derived based on the macrolayer dry-out model for critical heat flux. This correlation is shown to have very good agreement with available data for different forms of spray cooling. The second study deals with the heat transfer characteristics of a vertical array of heaters in a confined space in liquid nitrogen. Experiments were conducted to study the behavior of flush mounted heaters in a vertical array with limited space in front. The results show the effect of heater position, heater length, and the spacing in front of the heaters. The last part deals with flow boiling of liquid nitrogen from discrete heat sources in a rectangular channel. An experimental apparatus has been designed and fabricated to study the effect of various geometrical parameters in flow boiling from discrete heat sources.

**14. SUBJECT TERMS**

Cryogens, Spray Cooling, Pool Boiling, Heater Array, Flow Boiling, Critical Heat Flux, Confined Space, Liquid Nitrogen

**15. NUMBER OF PAGES**

55

**16. PRICE CODE**

| 17. SECURITY CLASSIFICATION OF REPORT | 18. SECURITY CLASSIFICATION OF THIS PAGE | 19. SECURITY CLASSIFICATION OF ABSTRACT | 20. LIMITATION OF ABSTRACT |
|---|---|---|---|
| Unclassified | Unclassified | Unclassified | SAR |

NSN 7540-01-280-5500

# TABLE OF CONTENTS

# LIST OF ILLUSTRATIONS

# NOMENCLATURE

d      diameter of a droplet in a spray sample, m

$d_{30}$      volume mean diameter of spray, $(\Sigma d^3/N_t)^{1/3}$, m

$d_{20}$      surface mean diameter of spray, $(\Sigma d^2/N_t)^{1/2}$, m

$d_{32}$      Sauter mean diameter of spray, $\Sigma d^3/\Sigma d^2$, m

$d_d$      diameter of the liquid disc formed by impinging drop, m

D      hydraulic diameter of heater surface, m

G      liquid mass flow rate per unit surface area, $kg/m^2.s$

$h_{fg}$      latent heat of vaporization, J/kg

l      vertical length of the heater, m

L      vertical length of the confined heater array, m

N      rate of droplets impinging per unit area,

        $N = 6.V/(\pi.d_{30}^3)$, $/m^2.s$

$N_t$      total number of droplets in the spray in a sample time

$P_a$      ambient pressure, $N/m^2$

$P_s$      stagnation point pressure of air flow field, $N/m^2$

q"      heat flux, $W/m^2$

$q"_c$      critical heat flux, $W/m^2$

s      spacing between the array and the confining plate, m

$T_w$      surface temperature, K

$T_{sat}$      saturation temperature, K

$u_b$      velocity of growing bubble surface, m/s

v      average spray droplet velocity, m/s

V      volume flow rate per unit area of heater, $m^3/m^2.s$

$\beta$      spreading ratio, $d_d/d_{20}$

$\delta$      initial macrolayer thickness, m

$\rho_l$      liquid density, $kg/m^3$

$\rho_v$      vapor density, $kg/m^3$

$\sigma$      surface tension, N/m

# 1. INTRODUCTION

The future of superconducting and low temperature MOS (metal-oxide semiconductor) electronics holds a great deal of promise. In some cases, the reductions in device sizes and the increased efficiency for liquid nitrogen temperature (LNT) operation may outweigh the cost. The most immediate applications will be in situations where a cryogenic liquid is readily available. In that case, the cryogen can be used as the heat transfer fluid and the size and weight of the onboard electronics can be reduced by an order of magnitude. However, the successful application of cryogenic cooling to electronics requires that the appropriate heat transfer characteristics be known. This is the main objective of this study.

The primary thermal management techniques for low temperature operation are spray cooling, pool boiling (immersion cooling), forced convection boiling (or flow boiling), and jet impingement cooling. This report which is the fourth annual report for the contract F33615-91-C-2152 focusses on spray cooling, pool boiling, and flow boiling.

Spray cooling was chosen as the first area of research because of its capability in removing large quantities of heat at very low liquid flow rates. Experiments were conducted for various spray cooling conditions using liquid nitrogen. The results of the experiments have been presented in previous annual reports for the contract [1-3]. Recently a new model for critical heat flux in spray cooling was developed. That model and the resulting correlations are presented in this report.

Pool boiling is the other heat transfer technique which is of great interest due to its simplicity. However, there are some concerns regarding the application of pool boiling in electronic devices containing multiple heat sources in confined geometries. In order to design compact devices, it is important to know the space limitations of the pool boiling technique. Thus, the second part of this study deals with the behavior of multiple heater arrays in liquid nitrogen and the influence of a confined space.

Flow boiling is another thermal management technique that has good potential in the cryogenic cooling area. The flow boiling characteristics of liquid nitrogen from discrete heat sources (as in electronic cooling) have not been studied previously. Hence, the last part of this study deals with the investigation of geometrical effects on the flow boiling characteristics of liquid nitrogen.

1

## 2. OBJECTIVES

The overall objective of this study is to obtain information on the heat transfer characteristics under conditions of cryogenic cooling in various modes. Also, the suitability of these heat transfer modes to aerospace applications has to be evaluated. Due to the lack of suitable design correlations/models, experimental studies have to be undertaken to evaluate the heat transfer characteristics of liquid nitrogen under pool boiling in complex geometries, spray cooling, forced convection boiling, and jet impingement. This would be followed by the development of design correlations for these modes of cooling. Finally, the applicability of these techniques to electronic cooling has to be demonstrated.

# 3. BACKGROUND

The electronic systems envisaged for operation at LNT fall into two categories. First, the superconducting circuits composed of high temperature superconducting (HTS) devices (switches, capacitors, inductors, etc.), and second, the hybrid circuits which contain both HTS and semiconductor devices. There are numerous applications for both types of circuits. These two configurations and their applications are discussed in the following sections.

## 3.1 Superconducting Circuits

Superconducting circuits will consist of HTS devices (logic gates, inverters, memory cells, etc.) with superconducting interconnects [4]. Almost all of the functions performed in high performance electronics can be done by a superconductor circuit [5]. However, superconductor circuits cannot handle high power levels; also, there are no superconducting rectifiers, and semiconductors make better amplifiers and mass memory devices. The main applications of HTS circuits will be

- High speed digital logic and memory: gate speeds under 10 ps are easily achievable using Josephson junctions [4,5] thus allowing the development of faster supercomputers;

- Far infrared/high frequency radar detection: with circuits employing Josephson junction device mixers, very-low-noise high-frequency detection (over 100 GHz) is possible with the only limitation being the Heisenberg uncertainty principle [4,6,7];

- Magnetic field sensors: very sensitive magnetometers and voltmeters made using SQUIDs (superconducting quantum interference devices) have application in magnetic field geophysical exploration and biomagnetic studies of the human body; and

- Superconducting-coil magnets and motors: superconducting-brushless-ac motors can be used in various applications.

## 3.2 Superconductor/Semiconductor Hybrid Circuits

MOS semiconductor devices show a marked improvement in performance as the operating temperature is lowered [5,8,9]. Furthermore, the thermal conductivities of semiconductor substrates and packaging materials (silicon, germanium, beryllium, alumina) are seen to increase dramatically as the temperature is lowered to LNT [10]. The main advantages of low

temperature operation are increased electron and hole mobilities, lowered interconnection resistivities, reduced leakage currents, greater subthreshold slope, and reduction in thermal noise. One of the possible applications of low temperature electronics will be in high efficiency ac/dc, dc/ac and RF power conversion at the multikilowatt level. As mentioned earlier, superconducting circuits are not capable of handling high power levels. Hence, MOS field effect transistors (MOSFETs) can be used with high Q inductors and capacitors made from HTSs to obtain the zero voltage switching circuits suitable for power conversion applications [9]. Such an integration will result in a drastic size and weight reduction. The efficiency of these circuits improves greatly at low temperatures due to the dramatic reduction in the on-resistance of power MOSFETs. However, the efficiency of these circuits depends greatly on the Q values of the inductors and capacitors used in the circuit. Hence, it is necessary to use HTSs for these components to obtain the maximum efficiency. Another application of hybrid circuits is the high-frequency receiver-signal processor [5]. Here, the devices best suited for each component of the circuit are used. Thus, a combination of superconductor and semiconductor devices provides a high performance circuit. In industry and transportation, the HTS ac motors employing MOSFET controllers have a variety of applications. The HTS-ac motors have been successfully tested recently and will be commercially available in the near future [11]. At the same time, locomotive engines using natural gas (stored at 110 K in liquid form) have been developed [12]. These two can be combined, with the liquefied natural gas acting as the coolant for the HTS motor and MOSFET switches, to produce a highly efficient and clean locomotive engine.

3.3 Thermal Management Issues

A cursory examination of heat transfer requirements in superconducting circuits may lead one to believe that due to the very nature of superconductivity heat dissipation would not be a problem. However, a closer examination reveals how ill-founded that notion is. The main components in a superconducting circuit are the high-speed low-power switches, the Josephson junctions (also called Superconductor-Insulator-Superconductor devices, SISs) [5,7]. The main advantages of these devices are the low gate delay times and low power dissipation; these features in combination will allow much higher device packing density compared to semiconductor circuits. However, the thermal management aspect of superconducting circuits at LNT has been of concern lately. A typical SIS working at 4.2 K has a power dissipation of

4

50 kW/m$^2$; however, for operation at 77 K, the same device may have a heat dissipation approaching 6000 kW/m$^2$ [13]. Obviously, this level of heat dissipation cannot be handled by common heat removal techniques. Hence, there are two options available for the thermal management of HTS circuits:

1. Immersion cooling (pool boiling) in liquid nitrogen (LN$_2$) with low device density packaging employing heat spreaders; and

2. High heat flux cooling with LN$_2$.

The first option cannot be expected to handle device heat dissipation above 500 kW/m$^2$. This is because the pool boiling critical heat flux for LN$_2$ is only about 160 kW/m$^2$ (calculated using Zuber model [14]). Hence, even with good heat spreaders, the overall device dissipation could not be expected to be more than 2-3 times this amount. Thus, immersion cooling will mean larger, and thereby slower, devices. This may not be a concern in some applications. However, for high speed digital applications, device sizes have to be kept as small as possible to minimize the distance travelled by the signal. In those cases, the second option of using a high heat flux cooling technique would be much more preferable.

The superconductor/semiconductor hybrid circuits are inherently more prone to thermal failure due to the presence of high heat dissipation transistors in the vicinity of superconducting elements. It is not possible to thermally isolate the superconductor and semiconductor elements because the interconnections themselves serve as thermal bridges. The successful operation of hybrid circuits depends on the ability of the cooling system to maintain the superconducting elements below their transition temperature. Hence, it is essential that the cooling system is capable of removing high heat fluxes from discrete locations (MOSFETs) to prevent any hot spots and the resultant system failure. Again, in this case, the choices are similar to the ones mentioned before.

Thus, the thermal management scenario in low temperature electronics consists of either using direct immersion pool boiling with heat spreaders, or, a high heat flux cooling technique. For the high heat flux situation, spray cooling is the technique which is of most interest because of its low liquid flow rate requirements. Low temperature spray cooling consists of subjecting the heat sources with a high speed spray of low temperature liquid. The two thermal management scenarios described above are shown in Figure 3.1. As shown in the figure, both scenarios require a refrigerator/condenser unless the low temperature liquid is available in abundance (as
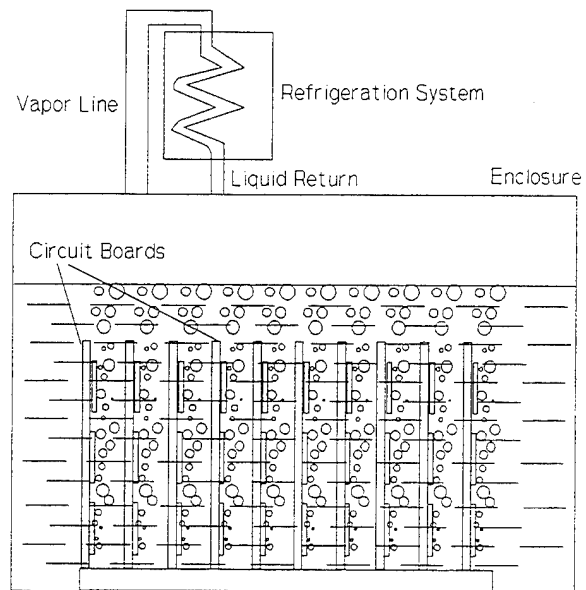
Immersion (Pool Boiling) Cooling
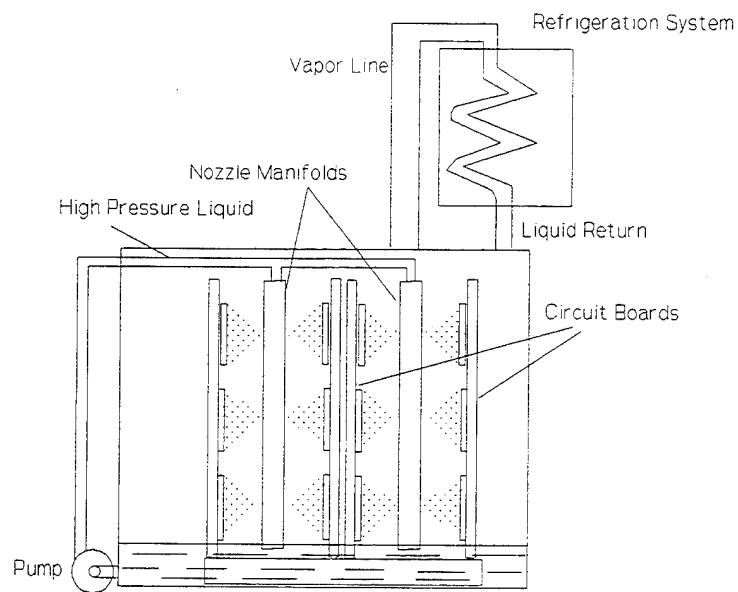


Spray Cooling System

Figure 3.1  Low Temperature Cooling Scenarios.

6

in the case of stored liquefied fuel). The spray cooling scenario will also require a pump for cases where a high pressure liquid is unavailable.

The main concern regarding these techniques is the lack of information about the heat transfer characteristics of cryogens under the particular conditions described above. Liquid nitrogen was selected as the cryogen for the heat transfer studies due to its suitability for both HTS and MOS devices. The heat transfer characteristics of spray cooling with liquid nitrogen were not available. Also, no general correlations were available for spray cooling. Thus, the spray cooling part of this study dealt with determining the heat transfer characteristics and obtaining suitable correlations. As mentioned earlier, the experimental data have already been presented in previous reports [1-3]. In this report, a new critical heat flux model and the resulting correlations are presented in Section 4. In case of pool boiling, the available correlations deal with simple situations only (e.g., single heater in an unconfined pool of liquid nitrogen). However, the conditions in electronic cooling are far more complex due to the interaction of various heaters and lack of space. Thus, the pool boiling part of the study dealt with the effects of multiple heat sources and confined space. The pool boiling study is presented in Section 5. The flow boiling study focusses on the liquid nitrogen flow boiling characteristics from discrete sources in a narrow rectangular channel. This study is in the early stages, and therefore, only the background and the experimental design are presented in Section 6 of this report.

7

# 4. CRITICAL HEAT FLUX IN SPRAY COOLING

## 4.1 Introduction

Although spray cooling has been used in industry (in continuous casting process, metal cutting process, etc.), the applications have typically involved very high surface temperatures (beyond the Leidenfrost temperature). At such high temperatures, the liquid cannot wet the surface. The momentum of the spray droplets enables them to get close to the surface and thus permits higher heat fluxes compared to direct immersion in the liquid. Hence, most of the research has traditionally focussed on spray cooling regime beyond the Leidenfrost temperature [15,16]. However, this regime is not of interest in electronic cooling because the device temperature has to be maintained low (typically < 85 °C).

Another regime of spray cooling which has been of interest in the past is the low spray density mist cooling. This form of spray cooling occurs when the number of droplets hitting the surface is small enough to prevent any interaction between the individual droplets. Thus, the heat transfer essentially occurs by evaporation/boiling in the thin liquid discs deposited by the droplets. The heat transfer phenomena in this case have been studied by Bonacina et al. [17]. This form of spray cooling is very efficient (i.e., almost all the liquid hitting the surface evaporates) but does not permit very high heat fluxes.

The high heat flux regime of spray cooling occurs when a dense spray is subjected upon a hot surface whose temperature is a few degrees above the saturation temperature of the liquid. Recently, significant research has been carried out for this form of low superheat high heat flux spray cooling. Chang et al. [18] have demonstrated the thermal management capability of spray cooling in MCMs. Pais et al. [19] showed that the efficiency and power input capabilities of laser diodes increase dramatically under spray cooled operation.

As with most processes involving phase change, the phenomena involved in spray cooling are very complex and not easy to model. Hence, most of the research has focussed on experimental investigation of the process [20-27].

Spray cooling can be broadly divided into two categories depending on the mode of spray generation:

1) Pressure atomization, where the high pressure liquid is atomized by the pressure differential across a nozzle.

2) Secondary gas assisted atomization, where a stream of high velocity secondary gas helps in atomizing the liquid into very fine spray; e.g. air brush.

The difference between the spray cooling physics for the two methods is caused by the presence of the secondary gas flow superimposed on the spray for the second method. Monde [21], Pais et al. [23], and Yang [25] among others, have studied spray cooling with an air atomizing nozzle. Studies employing pressure atomization have been reported by Toda [20], Choi and Yao [22], Cho and Wu [26], and Tilton [27] among others.

All of these studies have tried to deal with many aspects of spray cooling. However, all the studies focussed on a single liquid. In this study a semi-empirical general correlation for spray cooling is obtained using the macrolayer dry-out model. In the following sections this model and the correlation are discussed.


## 4.2 Experimental Evidence

Figure 4.1 shows the typical heat transfer characteristics for both modes of spray cooling. The characteristic curve for spray cooling with an air atomized water spray is shown in Figure 4.1(a) [25]. The curve can be divided into three clear regimes (shown in the figure):

I)   Single phase forced convection region marked by low heat transfer coefficient.

II)  Two phase boiling/evaporation region where the heat transfer coefficient is very high.

III) The flattening of the curve leading to dry-out at critical heat flux (CHF) (note: hereafter, dry-out of the surface and CHF are used synonymously).

The second part of the figure, Figure 4.1(b), shows the characteristic curve for spray cooling with pressure atomized water [27]. On comparing the two curves in Figure 4.1, it can be seen that the CHFs and heat transfer coefficients for the air atomized spray cooling are comparable to pressure atomized spray, although the liquid flow rate is more than 10 times lower. Although, the first case has a higher subcooling (80 °C compared to 5-10°C for the second case), the sensible heating can only account for a maximum of 1500 kW/m$^2$ (assuming the entire liquid flow is heated to the same level of subcooling as the second case).

Figure 4.1 shows that spray cooling permits exceptionally high heat transfer coefficients and CHFs for very low mass flow rates. Heat transfer coefficients higher than $2 \times 10^5$ W/m$^2$.K are easily obtained with water spray cooling. This is a tenfold improvement over pool boiling. Similarly, CHFs 5 to 10 times higher than pool boiling are achievable.

9
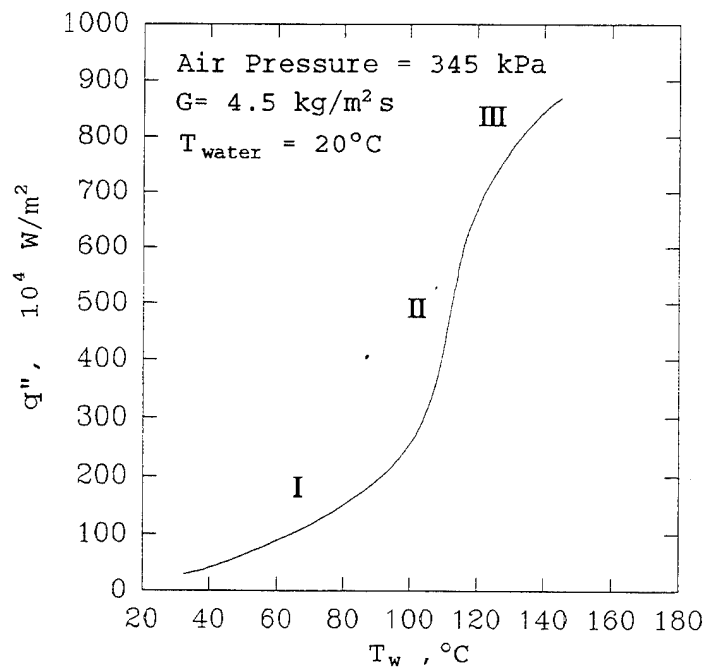
(a) Air Atomized Water Spray (Yang, 1993)
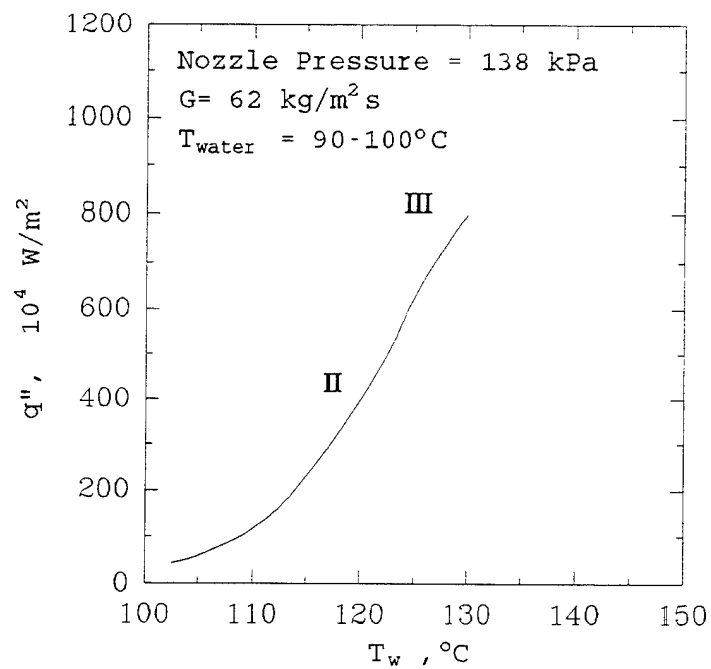


(b) Pressure Atomized Water Spray (Tilton, 1989)

Figure 4.1  Heat Transfer Characteristics of Spray Cooling

10

Some researchers have maintained that the CHF in spray cooling occurs due to the surface temperature approaching the Leidenfrost point [28,29]. However, as seen from Figure 4.1, the surface temperature is lower than the Leidenfrost temperature for water (about 150 °C). This is consistent with numerous other studies (e.g. References 20, 22, 23, and 24). Another point which can be noted from Figure 4.1 is that the CHF occurs although sufficient liquid is being supplied to the surface (i.e., some of the liquid goes unevaporated at CHF). Thus, the quantity of liquid supplied is sufficient to sustain a much higher heat flux.

In spray cooling, usually there is some splashing of the incoming spray. In most cases, the liquid loss due to splashing is relatively low. However, a study conducted by Tilton [27] to determine the cause of CHF found that as the heat flux was increased, the amount of liquid splashing off also increased dramatically. This was based on experimental measurements of the liquid influx and efflux obtained by a phase Doppler particle analyzer. Near CHF, the heat flux was found to correspond almost exactly to that expected from an energy balance assuming complete evaporation of the net liquid influx. Tilton attributed the increased splashing to the effect of bubbles bursting in the liquid film. The vapor inside the bubble escapes with a high velocity when the bubble breaks. Consequently, the liquid forming the upper layer of the bubble is expelled in this process. The escaping vapor may also entrain some incoming spray droplets.

In a study following the Tilton study [27], Yang [25] found only a slight increase in liquid splash off with heat flux. However, this was probably due to the fact that Yang used an air-atomizing nozzle. The strong air flow field entrains any droplets and inhibits splashing normal to the surface. Since only the liquid flux normal to the heated surface (near the center of the heater) was measured in Yang's study, any splashing liquid carried away by the stagnation air flow field was missed. Thus, Yang's observations were not necessarily contradictory to Tilton's.

The increased splash off could be due to two reasons: first, the bubbles bursting and expelling liquid as suggested by Tilton, and second, droplets entrained by escaping vapor. A simple calculation shows that for water, the average vapor velocity would only be 4.5 m/s at a heat flux of $6 \times 10^6$ W/m$^2$ (assuming all ensuing vapor flows normal to the heater surface). Since the droplet velocities are much higher (ranging from 10 to 50 m/s), it is unlikely that the vapor flux causes any significant entrainment. The first condition, where the bursting bubbles expel liquid from the film, is much more likely. Sehmbey et al. [24] suggested a macrolayer dry-out model based on this theory. This model and the resulting semi-empirical correlation is presented in the

following section.

## 4.3 Macrolayer Dry-Out Model

The macrolayer dry-out model for boiling systems was developed by Haramura and Katto [30]. They suggested that the CHF in boiling occurs when a thin macrolayer which is present below a large vapor bubble dries out before the vapor bubble can escape. The hypothesis for the dry-out condition for spray cooling is presented in Figure 4.2. As shown in the figure, the dry-out condition occurs in the following sequence:

1) increasing rate of bubbles production in the liquid film gives rise to a larger vapor bubble (which may last for only a few microseconds due to the high rate of bombardment by spray droplets)

2) this vapor bubble is broken due to an impinging droplet (or due to the excessive internal pressure) and the liquid forming the upper layer of this bubble is blown away by the vapor flow

3) the incoming droplets continue to wet the rapidly drying out surface. The dry-out will occur if the incoming droplets cannot wet the whole surface before the macrolayer dries.

The second stage of the process is supported by the observations of Tilton [27] mentioned earlier. The third condition is also supported by experimental evidence presented by Sehmbey et al.[24]. They showed that the CHF was a power function of the area wetted by the spray per unit time. This means that the CHF is a function of the rate of area wetted by the spray, not the overall liquid flow rate.

The dry-out condition can be written in mathematical form as Equation 4.1. Here $\delta$ stands for the initial macrolayer thickness, $d_d$ represents the average diameter of the disc formed by an impinging droplet ($d_d = \beta d_{20}$, where $\beta$ is the spreading ratio), and N is the number of droplets hitting a unit area per unit time. Thus, Equation 4.1 represents a balancing of the time required to wet a unit area and the time required to evaporate the macrolayer of thickness $\delta$ initially present on that area.

$$\frac{1}{N(\frac{\pi}{4}d_d^2)} = \frac{\rho_1 \delta h_{fg}}{q_c''} \qquad (4.1)$$

The difficulty in the application of the macrolayer dry-out model lies in the estimation of the
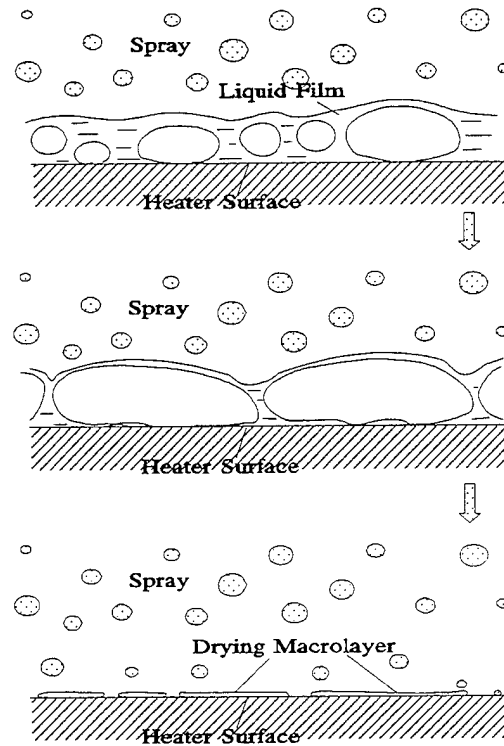
Figure 4.2 Macrolayer Dry-Out Model for CHF

initial thickness of the macrolayer. Haramura and Katto [30] obtained the macrolayer thickness based on the Helmholtz instability criterion for the vapor stems existing in the macrolayer. However, this situation does not seem very likely for very high heat flux cases. This is because the Helmholtz instability criterion indicates a very thin macrolayer (less than a micrometer thick if the Haramura and Katto model is used) for the heat fluxes encountered in spray cooling. Vapor stems (and instability in those short stems, if they exist) in such a thin macrolayer seem unlikely. Another model for initial macrolayer thickness was proposed by Kumada and Sakashita [31]. Their model is based on the lateral coalescence of the vapor bubbles on a heated surface. They obtained the initial thickness of the macrolayer based on a number of dimensionless parameters. However, their model resulted in a very involved expression (containing a number of empirically determined indices) for macrolayer thickness. An attempt to use their model for obtaining a general correlation for spray cooling CHF was not successful. In this study we use dimensional analysis to obtain the initial macrolayer thickness.

The macrolayer is formed by the lateral coalescence of small bubbles which go on to form

a bigger vapor layer which may exist for a very short time. Following the dimensional analysis of Kumada and Sakashita [31], and considering only the significant dimensionless parameters, the initial macrolayer thickness can be written in nondimensional form as Equation 4.2. The initial macrolayer thickness is related to the thickness of the liquid layer present below each individual bubble which finally make up the vapor layer. The first term on the right-hand side represents the ratio of the surface tension forces (which tend to keep the bubbles spherical) to the inertial forces (which act due to the rapid growth of the bubble and tend to keep the bubble in semispherical shape). The second term represents the density ratio, or the ratio of the mass

$$\frac{\delta}{R_b} = C \left( \frac{\sigma R_b}{\rho_1 R_b^2 u_b^2} \right)^i \left( \frac{\rho_1}{\rho_v} \right)^j \tag{4.2}$$

of liquid displaced by an equal volume of vapor. The terms $u_b$ (the velocity of the bubble surface), and $R_b$ (average radius of the bubbles which coalesce to form the larger bubble below which the macrolayer exists) are unknown. Regarding $R_b$, it should be noted that $\delta$ should not be dependent on $R_b$. This is because the CHF for different surface conditions was found to be almost the same at very different superheats. This means that the macrolayer thickness was similar although the nucleation conditions (and thereby the number of bubbles) were quite different. Thus, $\delta$ should be independent of $R_b$. As most of the surface area is covered by bubbles prior to CHF, the velocity of bubble surface can be considered to be proportional to the rate of vapor production per unit area; i.e., we can write: $u_b = C_1 . q_c'' / \rho_v h_{fg}$. Substituting this value of $u_b$ in Equation 4.2 and recognizing that $\delta$ should be independent of $R_b$, we can obtain Equation 4.3 which has only two unknown quantities j and $C_2$.

$$\delta = C_2 \left( \frac{\sigma}{\rho_1} \left( \frac{\rho_v h_{fg}}{q_c''} \right)^2 \right) \left( \frac{\rho_1}{\rho_v} \right)^j \tag{4.3}$$

Substituting $\delta$ from Equation 4.3 into Equation 4.1, we obtain the general form of the CHF correlation, Equation 4.4. The unknowns $\beta$ and $C_2$ are absorbed in $C_3$. This equation requires

$$\frac{q_c''}{\rho_v h_{fg}} = C_3 \left( \frac{\sigma}{\rho_1} N d_{20}^2 \right)^{1/3} \left( \frac{\rho_1}{\rho_v} \right)^k \tag{4.4}$$

data for only two different liquids ( i.e., two values of the density ratio) for obtaining k and $C_3$.

14

Here, the data for LN$_2$ and water were used. Both of these data sets involved horizontal heaters of 1 cm$^2$, the heater surface for the water study was square, while that for the LN$_2$ study was circular. The data from the R113 study were not used in developing the correlation since that study was performed on a vertically oriented surface [26]. It has been reported by Choi and Yao [22] that the CHF in spray cooling is dependent on the surface orientation. They found that the vertically oriented surface exhibited higher CHFs. There are very little data available for vertical surfaces; therefore, we limit this correlation to horizontal surfaces only. The probable reasons for higher CHFs from vertical surfaces are discussed later. The final correlation for CHF, obtained using LN$_2$ and water data, is shown in Equation 4.5. The comparison of the correlation to various data is shown in Figure 4.3.

$$\frac{q_c''}{\rho_v h_{fg}} = 0.31 \left( \frac{\sigma}{\rho_1} Nd_{20}^2 \right)^{1/3} \left( \frac{\rho_1}{\rho_v} \right)^{0.5}$$

(4.5)

where,

$$Nd_{20}^2 \equiv \frac{6 \cdot V}{\pi \cdot d_{32}}$$

It should be noted that the spreading ratio $\beta$ was assumed to be constant. This proved to be suitable for the range of data considered here, but it may not hold for very low droplet Weber numbers (all cases considered in this study had droplet Weber numbers exceeding 100). In the range of data considered in this study, no correlation between $\beta$ and the droplet Weber number could be found. Another point which can be noted is that the form of this correlation corresponds almost exactly to that obtained if Haramura and Katto's model for initial macrolayer thickness is used.

Although the R113 data were not used in obtaining the correlation, the data are only higher than the correlation by about 30%. This agrees with the fact that for a vertically oriented surface, the CHF is higher. The other data points are quite well compressed within a ±20% band. The reason for a vertical surface having higher CHFs is difficult to determine. It could be due to a number of reasons, among them: a vertical surface may have a thicker macrolayer; or, the liquid feed due to gravity may influence the CHF; or, some of the liquid blown away by exploding vapor bubbles may be re-entrained in the spray due to the horizontal orientation of the spray.

15

Cho and Wu [26] had successfully correlated their CHF data to the spray velocity. In fact, regarding all the data considered here, it is worth noting that the spray velocity, v, correlates the individual liquid data for $LN_2$ and R113 reasonably well (water data show only a weak dependence on v). However, the degree of dependence on velocity is different for each liquid, and thus, no general correlation involving the spray velocity was as successful as Equation 4.5. Furthermore, no theoretical basis for correlating spray cooling CHF with the spray velocity could be found; whereas, the CHF model presented before is quite reasonable.

Figure 4.3 shows the comparison of the correlation to various data including data for the air atomizing nozzles used in past studies. It should be noted that although only two data sets [24, 27] were used in deriving this correlation, it shows good agreement to the data sets of Toda [20], Cho and Wu [26], Pais et al. [23], Sehmbey et al. [32], and Yang [25].

It should be noted that the only spray parameter needed for this correlation is the Sauter mean diameter, $d_{32}$. This can be calculated from correlations provided by Lefebvre [33]. It should be noted that the exponent of $d_{32}$ in the correlation is only 1/3. This means that even a +100 % error in $d_{32}$ would only cause a 26% error in the predicted CHF value.

Referring to Figure 4.3, the data sets which involved air-atomized water spray (the last three sets), the trend shows some deviation from the correlation. This is due to the presence of the stagnation air flow field. The air flow field has a two fold effect. First, it will encourage the reimpingement of droplets blown away by the bursting bubbles. Secondly, it may increase the spreading ratio of the impinging droplets. Both of these factors cause the deviation from the correlation. The following section deals with the adjustments required for applicability to air atomized sprays.

## 4.4 General Correlation

In order to accommodate the effect of the air flow field, we introduce the nondimensional stagnation pressure, $P_s/P_a$, which is the ratio of the pressure at stagnation point of the air flow field to the ambient pressure. The main effect of the stagnation flow field is to create a squeezing force on the droplets hitting the surface (thereby increasing the spreading ratio $\beta$). As the stagnation pressure increases, this squeezing force will increase. Similarly, the possibility of the blown off liquid reimpinging the surface increases as the air velocity (proportional to the stagnation pressure) increases. Thus, the term $P_s/P_a$ was selected as the representative parameter
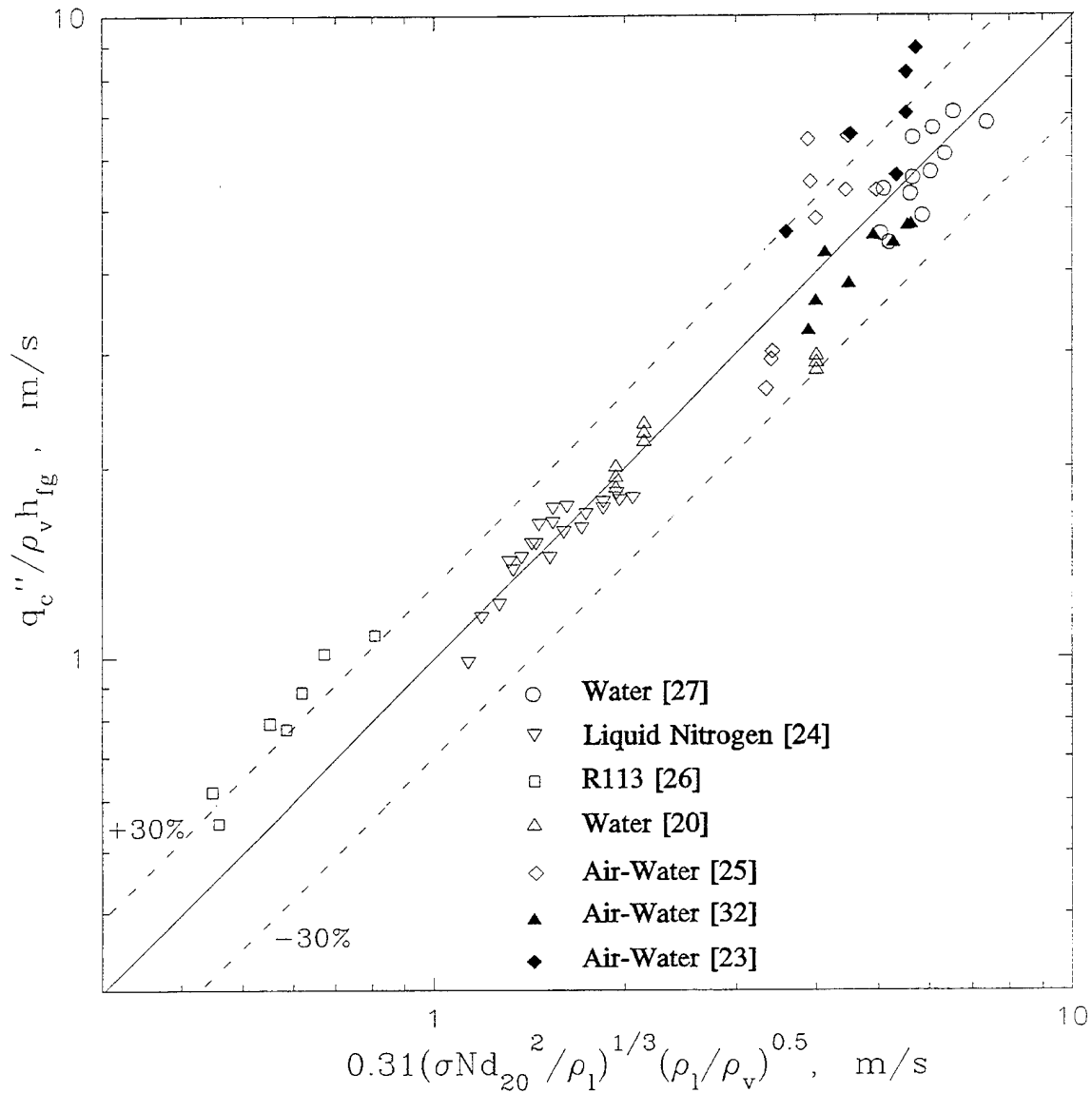
Figure 4.3 Comparison of Data to Equation 4.5

for the overall effect of the stagnation air flow field.

In most cases involving air atomizing nozzles, the nozzle to surface distance is more than 2 times the surface diameter (or length). In these cases the stagnation point pressure can be considered as the representative pressure for the flow field on the entire surface. The stagnation point pressure of the flow field was not measured in any of the studies. However, the stagnation point pressure of the flow field should be very close to the stagnation pressure in the nozzle since the nozzle was only 22 mm (approximately) away from the surface for all these studies.

17

Hence, the upstream air pressure can be substituted for the stagnation point pressure without a significant error. However, due to this approximation, the resulting correlation cannot be applied to situations where the distance between the nozzle and the surface is very large or where the surface is large and the nozzle is very close to the surface.

Introducing the nondimensional pressure ratio $P_s/P_a$ and determining the unknown exponent using data from the three sets involving air-atomized spray, we can write the general correlation for spray cooling CHF as Equation 4.6.

$$\frac{q_c''}{\rho_v h_{fg}} = 0.31 \left(\frac{\sigma}{\rho_1} Nd_{20}^2\right)^{1/3} \left(\frac{\rho_1}{\rho_v}\right)^{0.5} \left(\frac{P_s}{P_a}\right)^{0.25} \tag{4.6}$$

where,

$$Nd_{20}^2 \equiv \frac{6.V}{\pi.d_{32}}$$

In order to simplify and nondimensionalize this correlation, we substitute for $Nd_{20}^2$ and divide both sides by V. Rearranging the equation gives Equation 4.7 which shows the maximum efficiency of spray cooling (i.e., ratio of the CHF to the maximum possible heat removal) for saturated liquid. The comparison of this correlation to the data is shown in Figure 4.4.

$$\frac{q_c''}{\rho_1 V h_{fg}} = 0.38 \left(\frac{\sigma}{\rho_1 V^2 d_{32}}\right)^{1/3} \left(\frac{\rho_v}{\rho_1}\right)^{0.5} \left(\frac{P_s}{P_a}\right)^{0.25} \tag{4.7}$$

If we consider saturated liquids only, the maximum possible efficiency (as defined earlier) is expected to be 1.0. However, in most cases, there is some liquid loss due to splashing and some of the spray hitting outside the heating surface (near the edge). From Figure 4.4, it can be seen that the efficiency of the last three data sets (air atomized sprays) is very high. In most of these cases (i.e., the air atomized sprays), the liquid spray was in a subcooled state. This means that the Y axis does not really represent true efficiency (since subcooling is not accounted for). However, the subcooling can only cause a 10-20% deviation in these cases (this can be seen from Reference 32 where highly subcooled and almost saturated liquid were compared). The subcooling was not taken into account for this correlation for reasons explained later in this paper. Thus, even though subcooling accounts for a small part of this high efficiency, the air

18

atomized sprays are generally much more efficient as compared to pressure atomized sprays. This is due to the fact that air atomized sprays can be produced from very low liquid flow rate and consist of very fine droplets (i.e., very low $d_{32}$).

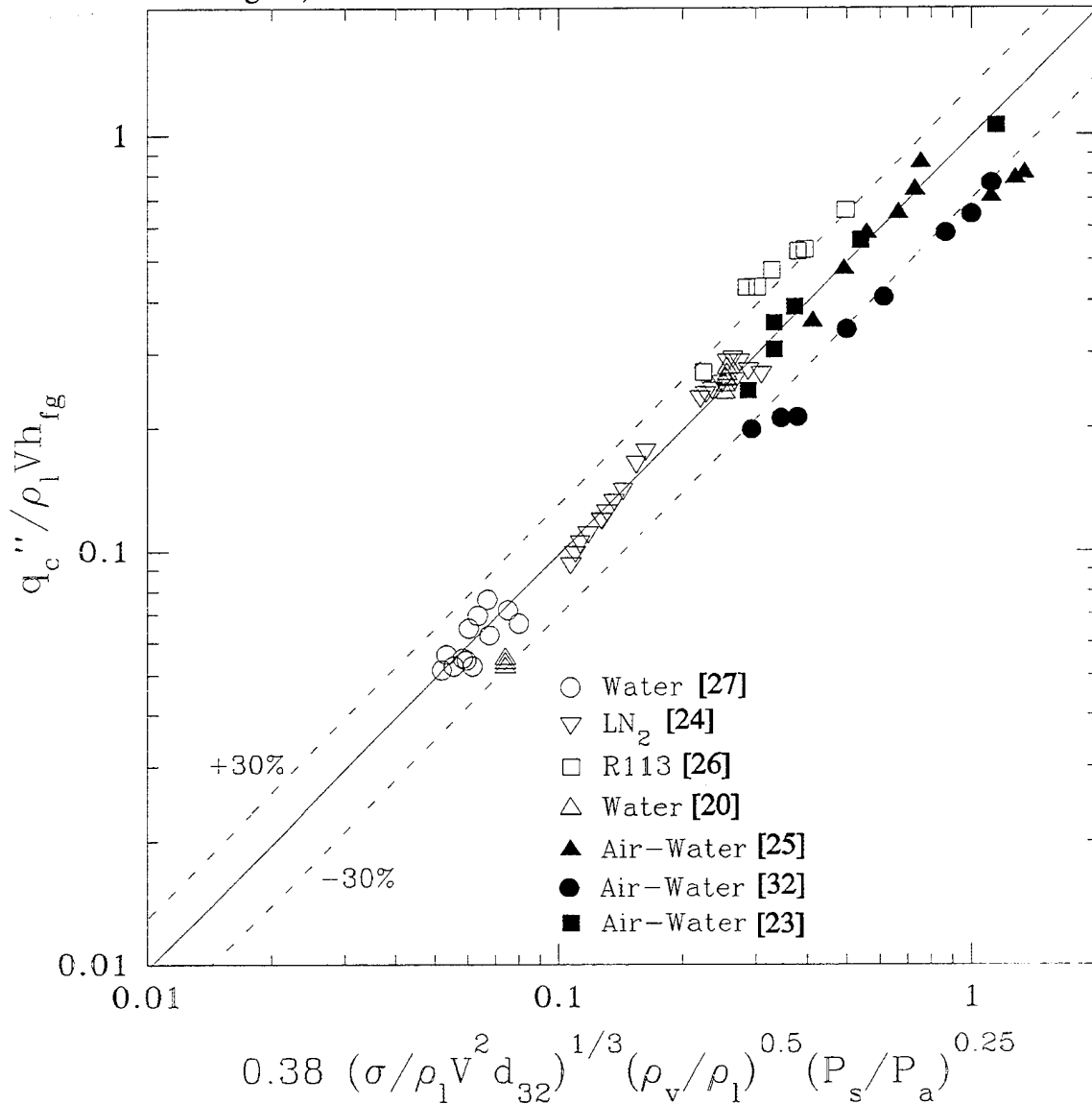As seen from the figure, the maximum deviation from the correlation is about 30% (for the



Figure 4.4  Comparison of General Correlation to Data

data of Cho and Wu [26]). The agreement of all the data to the correlation is quite good considering that some parameters (which differed in these studies) are not included in the correlation. These parameters and the reasons for excluding them are discussed in the following subsections.

### 4.4.1 Spray Nonuniformity

Most practical sprays have a large degree of nonuniformity in area coverage (i.e., the liquid flux on some areas is much greater than others). Unfortunately, there is little that can be done about this since all practical modes of spray generation lead to some form of nonuniformity. None of the studies have quantified this parameter. Thus, this correlation was based on an assumption of uniform spray distribution.

### 4.4.2 Liquid Subcooling

Some of the data sets considered here involved subcooled liquid. This was not taken into account while formulating the correlation due to two reasons. First, some studies did not report the subcooling [26]. Second, the data for subcooled liquids are insufficient for a satisfactory correlation. Thus, the correlation is mainly valid for slightly subcooled or saturated liquids.

### 4.4.3 Surface Properties

The surface roughness may have some influence on CHF in spray cooling with air atomizing nozzles. This was reported in studies by Pais et al. [23] and Sehmbey et al. [32]. The effect of surface roughness is not easy to quantify and the data on the effect of surface roughness are difficult to interpret. The reader is referred to Reference 24 for a better discussion on the effects of surface roughness. Here, it suffices to say that the CHF correlation presented here should be valid for normal surfaces (average roughness $R_a$ in the range of 0.1-0.6 $\mu$m).

Along with surface roughness, the oxide layer on the surface is an important factor. In most boiling systems, the presence of oxide layer can elevate the CHF substantially. All the studies considered in this paper used copper heating surfaces which were cleaned prior to each experiment. Thus, the presence of oxide layer in these cases could be ruled out.

### 4.4.4 Surface Material Properties

The thermal diffusivity of the heated surface is another property which influences CHF. Grigore'v and Dudkevich [29] studied spray cooling of $LN_2$ on different surfaces (unfortunately, they give no information on the liquid flow rates and spray parameters). They found that the CHF increased as the thermal diffusivity decreased. The increase in CHF was as much as 50% when comparing a silver surface and a steel surface. As mentioned earlier, all other studies used

copper heaters, therefore, there are no additional data on these effects.


4.4.5 Heater Size

The heaters in the studies considered here varied from 81 mm$^2$ to 330 mm$^2$. This a relatively small range of sizes. Hence, there was no apparent effect of the surface size. However, according to the dry-out model presented earlier, a large surface would allow the blown off liquid to return to the heater surface. This may increase the CHF for large surfaces. It is not clear that this effect would be significant given the fact that the returning liquid droplets would be very slow and may be entrained in the vapor flow. The surface size at which this effect would become significant is not known.

# 5. POOL BOILING FROM A VERTICAL HEATER ARRAY IN A CONFINED SPACE IN LIQUID NITROGEN

## 5.1 Introduction

Though extensive studies have been conducted on pool boiling of $LN_2$, they have mostly featured conventional pool boiling situations, i.e., single heat transfer surface in a pool of liquid [34,35]. The situation in most electronic equipment, however, is a series of discrete heat sources which may interfere with the boiling phenomena on each other. Some researchers have speculated that the bubble layer generated by the presence of numerous heat sources on a vertical plate may create less favorable boiling conditions for the upper heaters [36]. However, the recent study conducted by Chui et al. [37] to study these effects in $LN_2$ pool boiling showed that the heat transfer from the upper heaters was in fact enhanced when a lower heater was operating. In that study, the space in front of the heater array was large enough to prevent any distortion of the flow field. However, if the space in front of the array is reduced significantly such that the vapor flow from the lower heaters is forced against the upper heaters, a different result may be expected.

The effect of a very limited space in front of a heated plate in pool boiling with water has been studied in great detail by Fujita et al.[38]. They showed that as the space in front of the plate was reduced to below 2 mm, the critical heat flux (CHF) decreases while the heat transfer coefficient generally increases. This is because the pressing of the vapor bubbles against the heater permits a very thin film to exist between the vapor and the heater surface which in turn causes the heat transfer coefficient to increase. At the same time, the decrease in space causes greater resistance to liquid/vapor flow, thereby reducing the CHF. However, Fujita et al. studied the pool boiling behavior of only a single heater with water.

A few studies dealing with vertical arrays in pool boiling were also found. You et al.[39] studied pool boiling heat transfer in room-temperature gas-saturated FC-72 from a 3 x 3 array of 5 mm x 5 mm heaters. A confining plate was placed in front of the array at a distance of 2.3 mm. They found that boiling from a lower heater resulted in a decrease in the superheat overshoot (associated with boiling incipience in highly wetting liquids) at the upper heater. They found no consistent trend in the effect of lower heater on the heat transfer coefficients from the upper heaters. Also, they did not observe any significant effect of the lower heater on the CHF

from an upper heater. Another study, by Polentini et al.[40], involved nucleate boiling investigation from a 3 x 3 array (each heater 12.7 mm x 12.7 mm) in an enclosure containing FC-72 with two cold plates (maintained at 25 °C, 20 K below saturation temperature), one opposite to the heater array and one on top. They reported a 15% increase in heat transfer coefficient from the middle heaters when the array was vertically orientated. This was attributed to bubble pumped convection. However, the uppermost row of heaters had a lower heat transfer coefficient. This was attributed to vapor accumulation near the top of the array. Although they did not study the CHF conditions in detail, they reported that the CHF generally occurred at one of the heaters in the lowest row.

In these studies, the spacing in front of the heaters ($s$) was not changed. Thus, there is a lack of information on the effect of $s$ on heat transfer from an array of heaters.

This study was undertaken to investigate and quantify the effect of $s$ in pool boiling from a vertical heater array in $LN_2$. In addition, data was obtained for single heat source for comparison. The following sections provide a description of the experiments and the results for the areas of interest.

## 5.2 Experimental Setup and Procedure

This study involved experiments for pool boiling heat transfer from a 3 x 3 vertical array of heaters. Figure 5.1 shows the heater array; the heaters are mounted flush to the surface of the plate. The bare chip size in electronics range from 5 mm x 5 mm to a few hundred square mm. The CHF in pool boiling from vertical surfaces in $LN_2$ is around $1.45 \times 10^5$ $W/m^2$. This heat flux is modest, and therefore, many chips operating at $LN_2$ temperature will require heat spreaders much like those in use for room temperature operation. Hence, the size of the heaters was chosen close to the commonly used chip sizes; each heater in the array was 21.6 mm x 17.4 mm. The heaters have a sandwich construction. An oxygen-free copper heater block with an E-type thermocouple soldered at the center is soldered onto a ceramic substrate which has a thin resistor film deposited on its other face. Thus, the heat is provided by the film resistor and the temperature at the center of the heater is measured by the E-type thermocouple. The details of heater construction are provided in Reference 10.

Nine of these heaters were mounted flush to a thin stainless-steel plate which was bolted onto the heater module casing. The heaters were insulated on the back with closed-cell foam
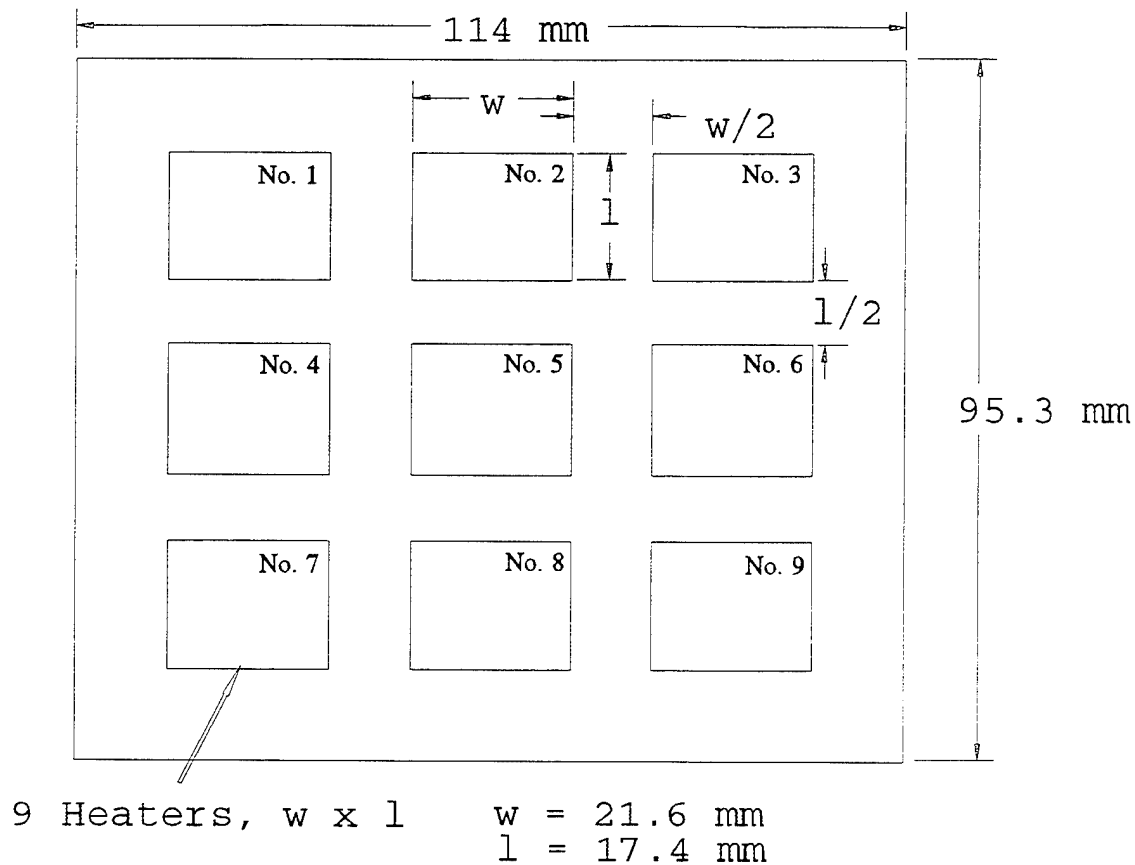
Figure 5.1 Heater Array

insulation. A low conductivity epoxy provided the seal between the stainless-steel plate and the copper heater blocks. The heater and thermocouple leads pass through an opening in the back of the module. The feedthrough hole is thoroughly sealed with closed cell foam to prevent liquid leakage into the module. The power input to each of the heaters could be individually controlled. The heater module allows for the installation of an acrylic plate facing the heaters. Four spacers (at each edge) serve to maintain a uniform space in front of the heaters. The space between the heater plate and the confining plate could be varied by using spacers of different thicknesses.

Figure 5.2 shows the details of the experimental setup. Experiments were conducted in a seamless glass (borosilicate) cylinder with an inner diameter of 190.5 mm, and a height of 254 mm. It contained a pool of $LN_2$ during the experiment. To prevent heat transfer from the environment, and allow for visualization of the boiling phenomena, this cylinder was placed inside another glass cylinder with inner diameter 240 mm. During preliminary experiments, it

24

was seen that the cool-down time for the whole system was too long. Hence, a 150-mm-ID borosilicate beaker was placed inside the inner chamber, the whole chamber filled with $LN_2$ and the heater module placed in the beaker. After this adjustment, the liquid pool inside the beaker became stagnant very quickly and this allowed for more efficient operation. The experiments were conducted at atmospheric pressure. The opening on top of the chamber (50 mm in diameter) allowed for liquid refilling, heater and thermocouple wire feed-through, and vapor exhaust. The vapor exhaust flow was always enough to prevent any back-flow of room air (and moisture) into the chamber. Thus, any ice formation inside the chamber was avoided.
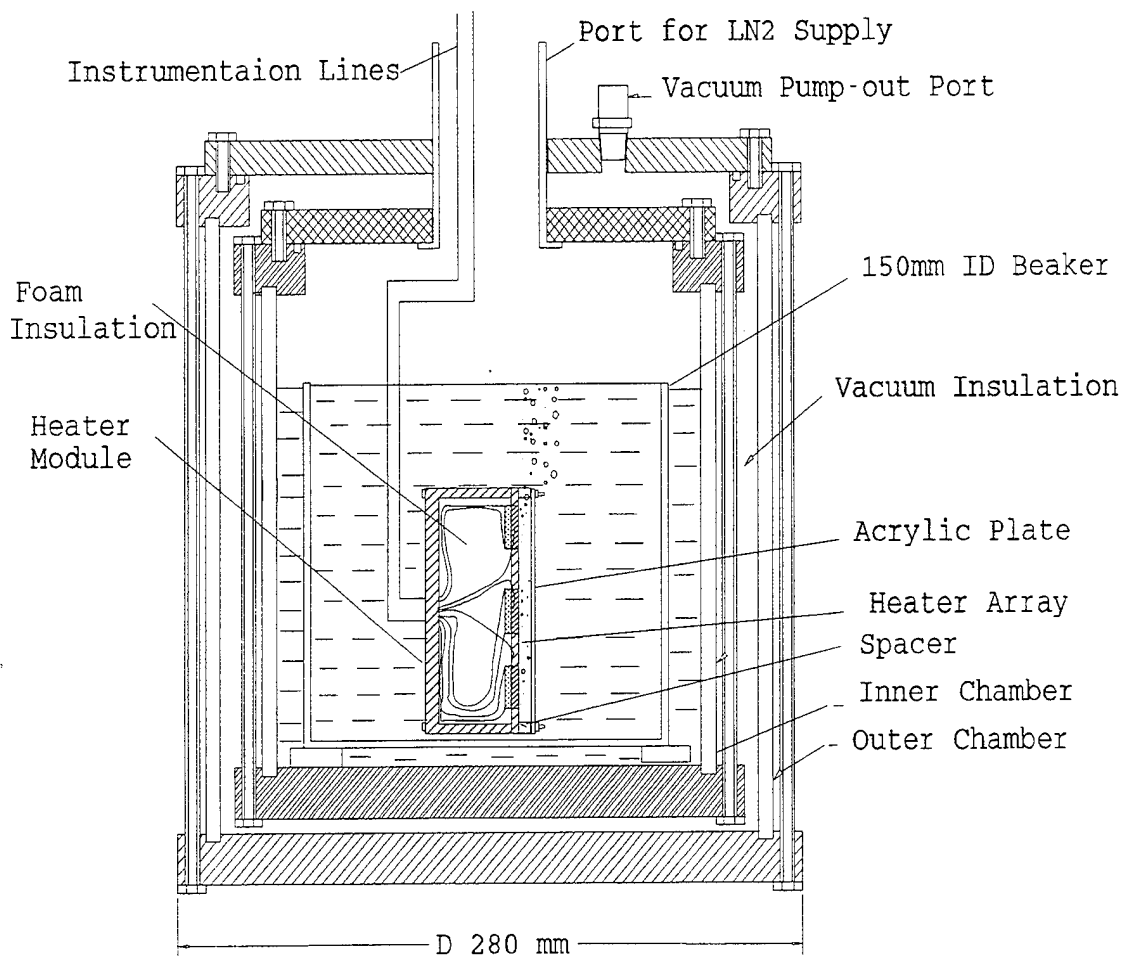


Figure 5.2 Experimental Setup

Before collecting each set of data, the heater surfaces were cleaned with dilute hydrochloric acid and deionised water to remove any oxides. The surface roughness of the heaters was measured by a surface profilometer. All the surfaces had average roughness $R_a$ of around 0.15

$\mu$m.

Prior to putting the heater module in the experimental chamber, a specific gap for the confining plate was set by installing the appropriate spacers. For each plate spacing, two types of experiments were conducted. First, the heat transfer characteristics for the whole array were determined. This was done by applying the same voltage across each of the resistance heaters and slowly increasing the voltage till CHF was observed on any of the heaters in the array. CHF was evidenced by a rapid increase in temperature for that particular heater. After each step increase in voltage, sufficient time was allowed for all the temperatures to reach a steady state. The second type of experiments involved determining the heat transfer characteristics of individual heaters. This was done in a similar manner except for the fact that the voltage was applied to only one heater at a time. This way, the heat transfer characteristics of any heater while working in the array, or individually, could be determined.

After each experimental run, the pool of $LN_2$ was replenished to maintain a constant level. The decrease in liquid level during an experiment was never more than 2-3 cm. During the experiment, all data, such as heater temperature and power dissipation, were collected by an IBM PC 386 through a programmed Hewlett Packard 3852A Data Acquisition/Control Unit.

Since the heater module and the heaters were rectangular, experiments were conducted for both vertical orientations to investigate the influence of inter-heater distance and heater dimensions. In addition, the reproducibility of the data was determined by repeating some of the experiments. It was found that the heat transfer curve and the CHF were reproducible within the experimental uncertainty limits mentioned in the following section. The only data which were not reproducible were the temperature overshoots (typical of highly wetting liquids) prior to onset of nucleate boiling when only one heater was operating.

## 5.3 Uncertainty Analysis

The complete details of the uncertainty analysis can be obtained from Reference 10. The overall uncertainties are provided here. The uncertainty in measured heat flux $q''$ was less than $\pm 3\%$. The maximum uncertainty in superheat $\Delta T$ was $\pm 0.44$ K. The uncertainty in determining the CHF $q_c''$ was the greater of $2.5 \times 10^3$ W/m$^2$ and $\pm 5\%$.

The uncertainty in the spacing $s$ is related to the flatness of the acrylic plate and the heater plate along with the uncertainty in the spacer thickness. Taking this into account, this uncertainty

was $\pm 0.05$ mm.

## 5.4 Results and Discussion

The results for the single heater are discussed first. A set of data was initially obtained without the confining plate in place. This served as the reference data set for open pool boiling. A total of seven different spacings were tested ($s$=0.3, 0.7, 1.0, 1.6, 3.2, 4.8, and 6.4 mm). Figures 5.3 and 5.4 show the heat transfer characteristics for heater 2 (the top heater in the middle column) at different plate spacings. Figure 5.3 shows the heat transfer curve for relatively large gaps ($s \geq 3.2$ mm). At these gaps, the bubble flow is not greatly affected by the presence of the confining plate. As seen from the figure, the data at low heat fluxes are nearly identical for open pool boiling and for these gaps. However, as the heat flux is increased, the bubble flow becomes significant and is forced against the heater due to the presence of the opposing plate. This allows heat transfer to occur through a thin liquid layer present between the vapor and the heater surface. Thus, the boiling curve for the lower values of $s$ shifts a little to the left at high heat fluxes.

As the confining plate is moved closer, the effect of confined space becomes more evident. As the spacing $s$ decreases, the bubbles growing on the surface become deformed and cover large areas on the surface. Thus, the initiation of nucleate boiling anywhere on the surface leads to high heat transfer coefficients as these deformed bubbles move over the heater and permit evaporation across a thin liquid film. As shown in Figure 5.4, the heat transfer coefficient increases greatly at low heat fluxes as $s$ is decreased below 1.6 mm. In the study by Fujita et al. [38], they observed that the boiling curve shifts to the right when the spacing is reduced to 0.15 mm. They attributed this decrease to the fact that most of the heater surface dries out very early and the heat transfer takes place mainly at the heater edges. This shift (to the right) in the boiling curve was not observed in the present study.

As the heat flux is increased, the deformed bubbles due to different sites coalesce. As these coalesced bubbles begin to cover most of the surface, the heat transfer coefficient begins to stabilize. This causes the slope of the curves to decrease at higher heat fluxes. The narrow spacing slows down the vapor removal and liquid supply, thereby lowering the CHF. Thus, the CHF value decreases dramatically as $s$ is decreased. At a spacing of 0.3 mm the CHF is just
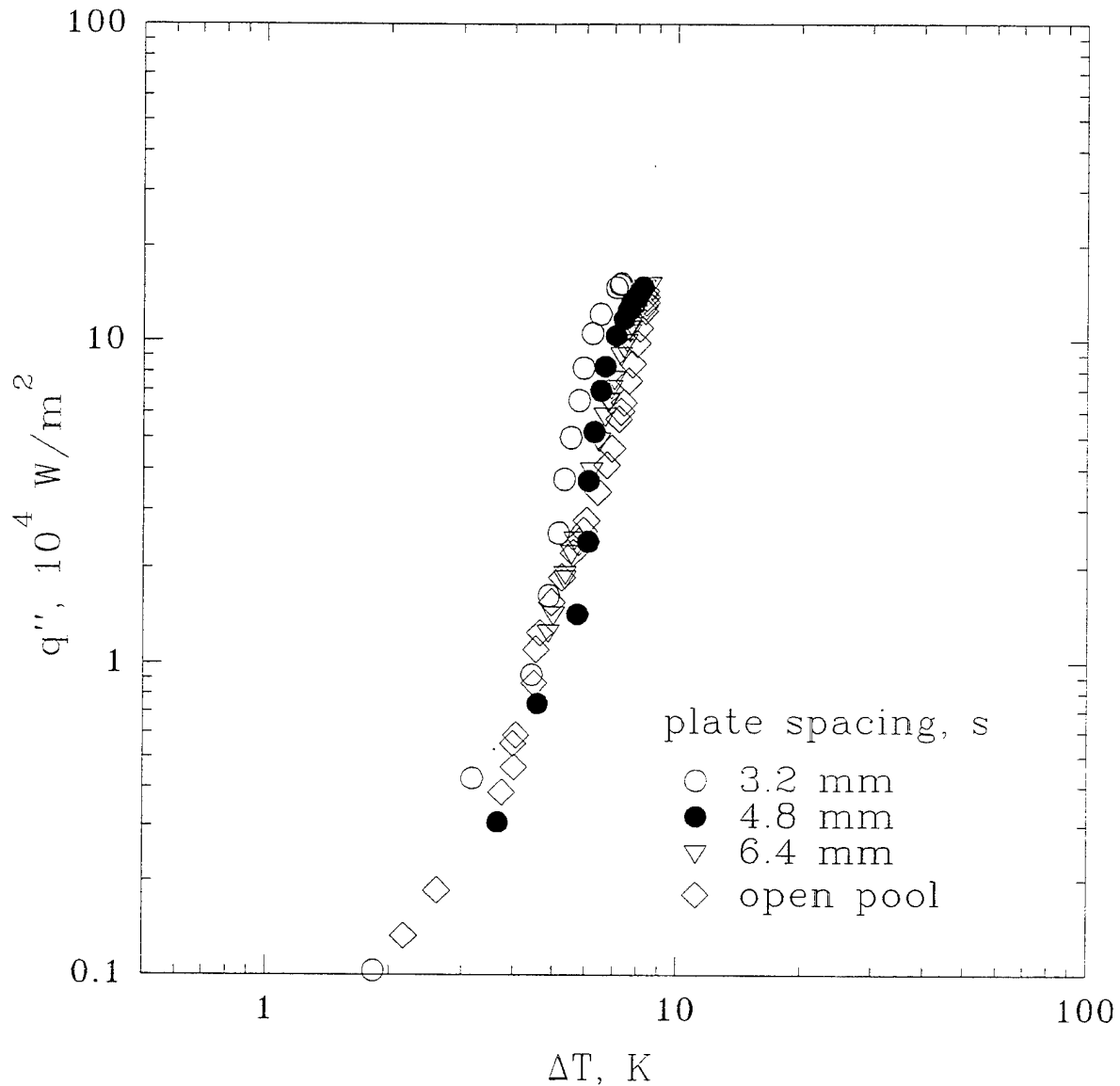
Figure 5.3 Heat Transfer Characteristics for Large $s$

$3.2 \times 10^4$ W/m$^2$ (compared to $1.45 \times 10^5$ W/m$^2$ for unconfined pool boiling).

## 5.4.1 Effect of Heater Position

The behavior of other heaters operating alone was qualitatively similar to the results shown in Figures 5.3 and 5.4. However, the lower heaters had higher CHFs for the two smallest gaps ($s = 0.3$ and 0.7 mm). This is due to the lower distance between the heater and the lower edge of the confining space. This decreases the length the liquid has to travel through the narrow gap in the upward direction to get to the heater. Figure 5.5 shows the comparison between heater
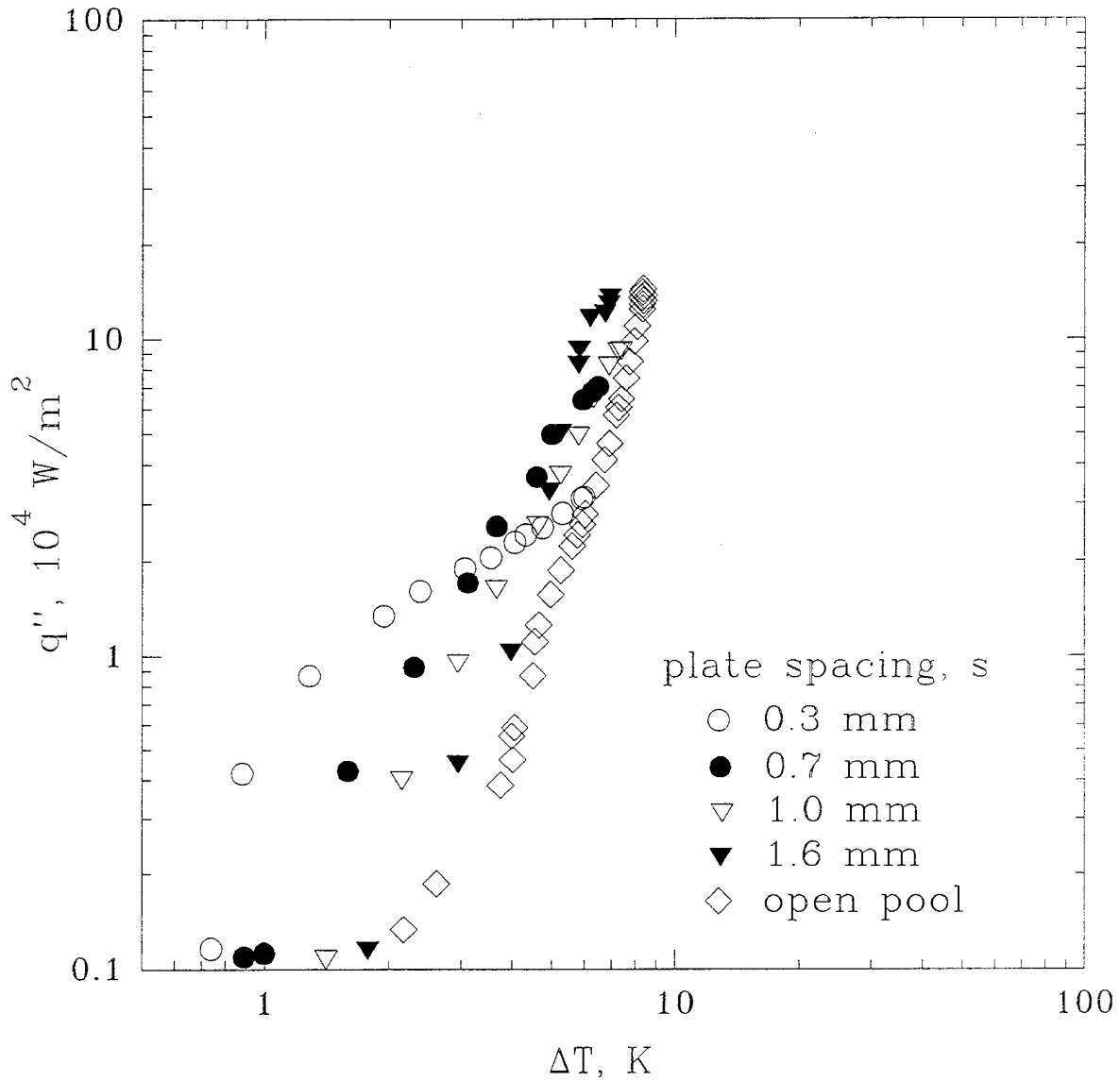
28

Figure 5.4 Heat Transfer Characteristics for Small $s$

2 (top of the middle column) and heater 8 (bottom of the middle column) for two different spacings for the short orientation. As shown in Figure 5.5(a), the two boiling curves are nearly identical for $s= 1.0$ mm. At $s= 0.7$ mm (Figure 5.5(b)), the heat transfer curves are still close. However, the CHF for the lower heater (heater 8) is about 25% higher. For $s=0.3$ mm (not shown here), the CHF for heater 8 was nearly 50% higher than heater 2.

The middle column of the array was the main focus of the study because its behavior would be close to the behavior of an inner column in a larger array. However, the heat transfer characteristics of the heaters in the outer columns were also studied. Generally, the boiling

curves were quite similar to those presented in Figures 5.3 and 5.4. For the two narrowest spacings ($s$=0.3 and 0.7 mm), the CHFs for the side heaters were up to 15% higher as compared to a middle heater in the same row. This is also due to the closeness of one edge of the heater surface to the edge of the confining space.

## 5.4.2 Effect of Heater Length

The geometry of the heaters allowed for two values of heater length (17.4 and 21.6 mm). There were no significant difference in the heat transfer curves for the two orientations. However, the CHFs for heaters in corresponding locations were usually lower for the longer heater length at larger values of $s$ ($s \geq 1.6$ mm). This is to be expected because longer heaters usually show lower CHFs [38]. For the three smallest values of $s$ ($s$= 0.3, 0.7, and 1.0 mm), the CHF does not show any appreciable dependence on the heater length. At these values of $s$, the CHFs for individual heaters in both orientations were within the range of experimental uncertainties.

## 5.4.3 Heat Transfer from the Array

The heat transfer characteristics of all the heaters were obtained while the whole array was operating. These were compared with the heat transfer characteristics for those heaters operating individually. For the two largest values of $s$ (4.8 and 6.4 mm), the heaters in the bottom row had the same characteristics as they had when operating alone. At these spacings, the top and the middle row heaters had higher heat transfer coefficients at low heat fluxes (less than $2\times10^4$ W/m$^2$). This is due to the flow field induced by the bubbles generated at the lower heaters.

As the spacing was reduced, the bottom row heaters started to be affected due to the thermosyphon effect and had higher heat transfer coefficients at low heat fluxes. At the four smaller spacings (0.7, 1.0, 1.6, and 3.2 mm), all the heaters were affected due to this effect. This is shown in Figure 5.6 which is a comparison of heater 2 operating alone, and, with the array operating at the same heat flux.

Here, it should be mentioned that the CHF for the array means that one of the heaters in the array dries out when the heat flux is increased beyond this value. For plate spacings larger than 1.6 mm, the heater to dry out was usually in the lowest row. This is similar to the results reported by Chui et al. [37] for unconfined pool boiling. The CHF occurs in lowest heaters

30
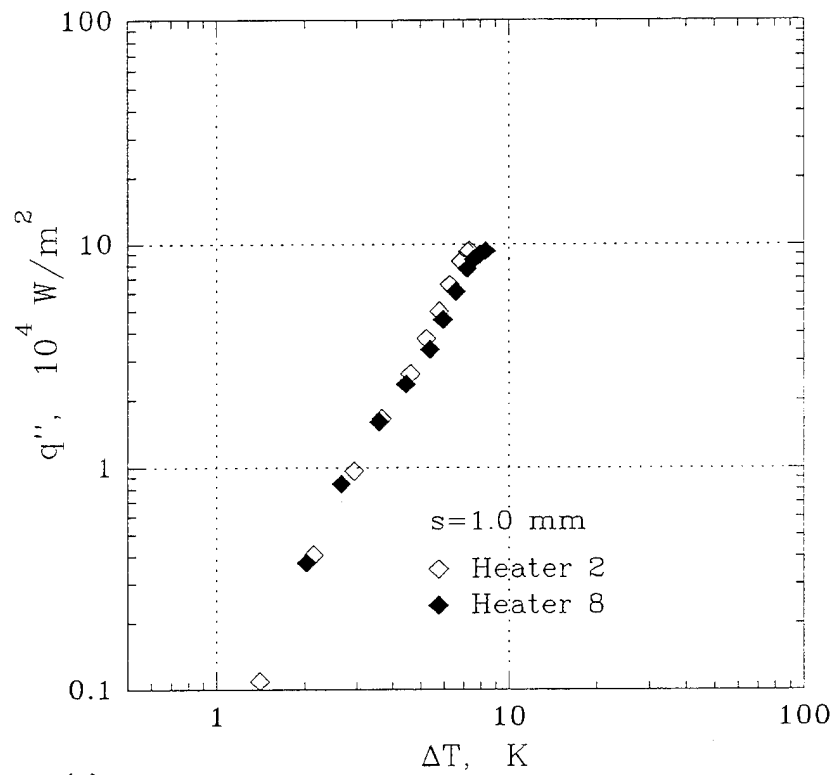
(a)
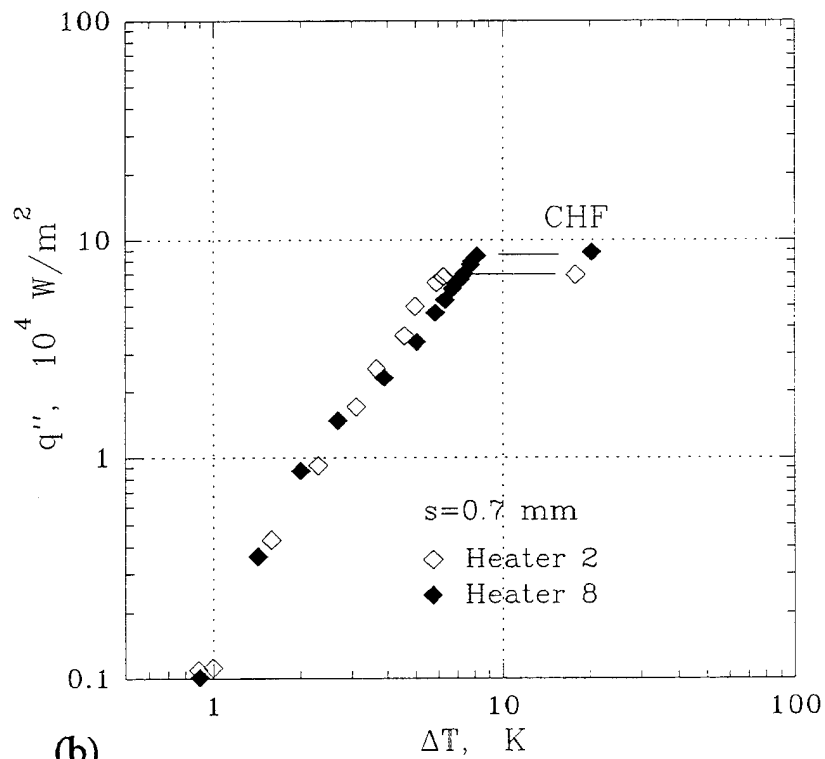


(b)

Figure 5.5 Comparison of Top and Bottom Heaters

31

because the flow caused by the bubble generation on the lower heaters elevates the CHF from the higher heaters. For $s = 1.6$ mm, the two orientations of the array gave different results. For the tall orientation, heater 4 (top heater in middle column) dried out first. But, for the short orientation, a lower heater dried out first. However, for the lowest three values of $s$ (0.3, 0.7, and 1.0 mm), the CHF always occurred on the top most heater in the middle column. This means that the vapor fraction has more influence on the CHF as the confining space is reduced.

As shown in Figure 5.6, as $s$ is decreased to 1.0 mm, the difference between the heat transfer curve for the heater operating alone and in the array becomes less significant. The maximum difference between the two curves was for the spacings of 1.6 mm and 3.2 mm. As the spacing was reduced below 1.6 mm, the difference between the two cases diminished. For the minimum spacing of 0.3 mm, the two curves are essentially the same at lower heat fluxes. However, the array has a lower CHF. This is due to the higher vapor fraction at the upper heaters.

The effect of the high vapor fraction on CHF is not as bad as expected. In fact, the worst degradation of CHF was about 30% (for the lowest $s$ in the tall orientation). The CHF data are discussed in more detail in the following subsection.

5.4.4 Critical Heat Flux

The CHFs for the top heater in the middle column for both orientations of the array are shown in Figure 5.7. As mentioned earlier, the CHFs for the tall orientation (longer heater length) are slightly lower for plate spacings of 1.6, 3.2, and 4.8 mm. The figures also show that the differences in CHF for the array and the heater operating alone are fairly small for both orientations.

In a previous study, Monde et al.[41] proposed a general correlation for CHF from heaters in narrow vertical channels. As reported by them, their correlation did not agree with data for liquid helium. They did not have access to any data for $LN_2$ in similar geometry. Thus, their correlation was untested for $LN_2$. The correlation is in nondimensional form with the CHF being proportional to $1/(1 + C(l/s))$ ($C$ depends on the liquid). The ratio $l/s$ has been used by many researchers in the past to correlate the CHF data from heaters in confined spaces. It has been shown that for $l/s$ lower than 10, the CHF is similar to that in unconfined pool boiling. For higher values of $l/s$, a number of empirical correlations (usually limited to the liquid of interest) have been proposed [41].

32
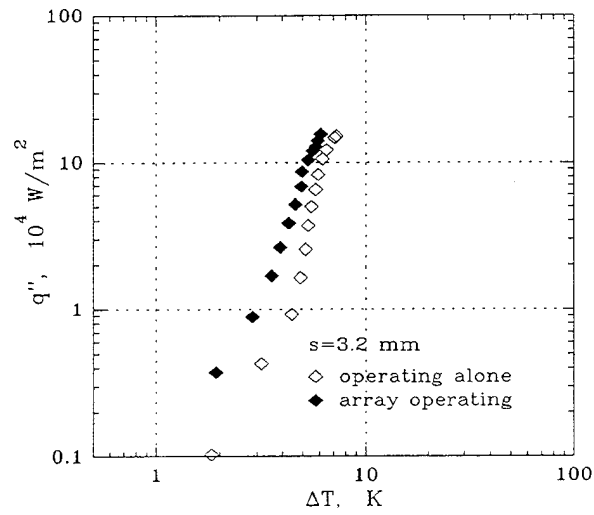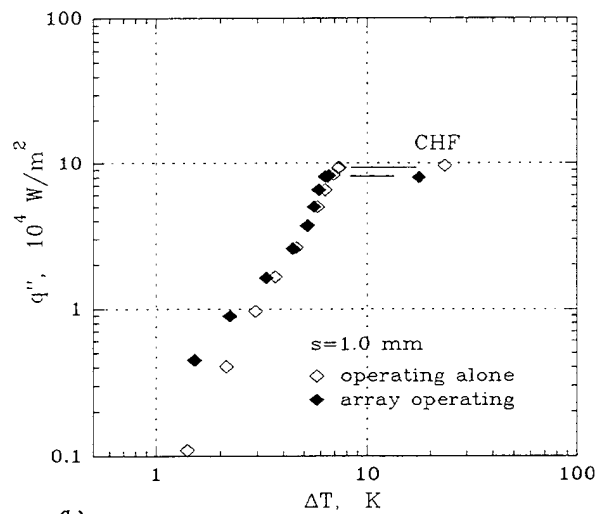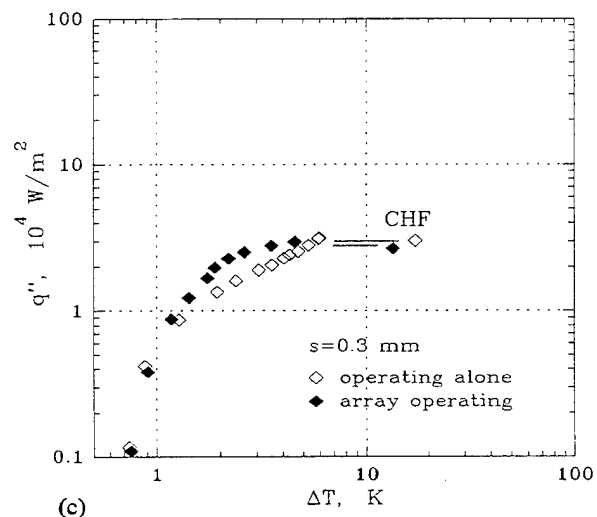
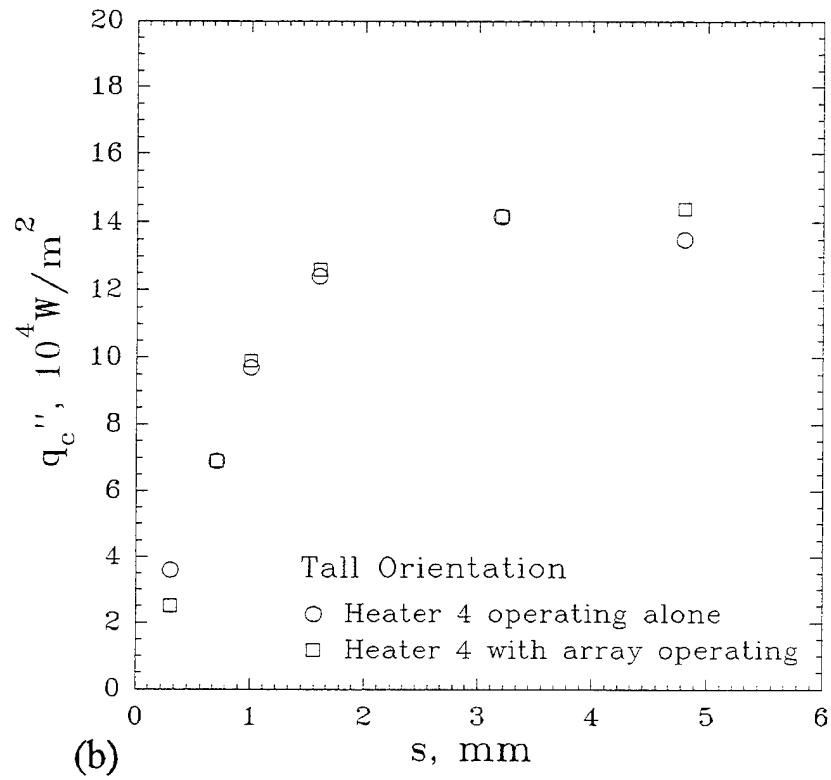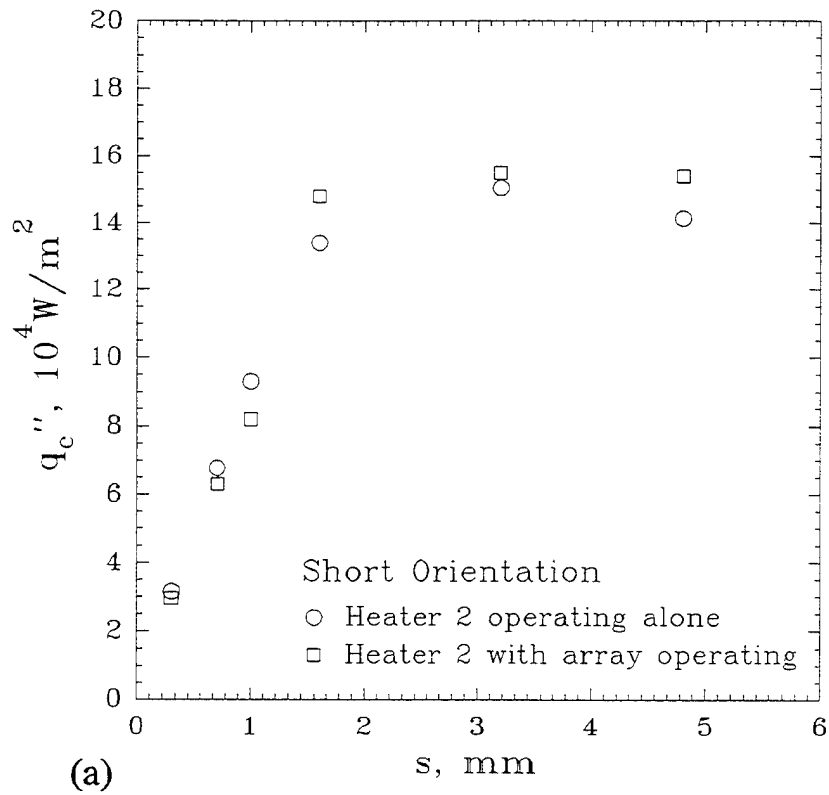Figure 5.6 Effect of the Heater Array

Figure 5.7 Variations in CHF

34

The general correlation derived by Monde et al. [41] is mainly applicable to a single vertical heater with a similar size confining plate opposite to it with the periphery closed on the sides. The main geometrical parameter in the correlation is the heater length to the spacing ratio $l/s$. However, in this study, the heater sizes were considerably smaller than the size of the confined area and the confined area had an open periphery. In this case, the correlation does not work very well if the heater length is used in the ratio. This is because the liquid has to go through a long narrow gap before reaching the particular heater. In addition, the vapor also has to escape through a narrow gap longer than the heater length. These factors are not accounted for in the aforementioned correlation. However, since the focus of this study was on the behavior of the array, it is more useful to obtain a correlation for the array CHF.

For heater arrays, usually the worst case prediction of CHF can be obtained by assuming that the entire array forms a single heater with a uniform heat flux. In the present study, this would mean that a worst case CHF for the array can be obtained by substituting the vertical length of the confined array ($L$) in place of heater length ($l$) in the CHF correlation. Referring to Figure 5.1, $L$ would be 95.3 mm for the short orientation and 114 mm for the tall orientation. Using the length $L$, the correlation of Monde et al. can be written as Equation 5.1. However, the effect of the open side periphery is not taken into account in this correlation.

$$\frac{q_c''/\rho_v h_{fg}}{(\sigma g(\rho_l-\rho_v)/\rho_v^2)^{1/4}} = \frac{0.16}{1+6.7\times10^{-4}(\rho_l/\rho_v)^{0.6}(L/s)} \tag{5.1}$$

As shown in Figure 5.8, comparing Equation 5.1 to the data indicates that the correlation is quite close to the data for the array CHF. It can be seen that the tall orientation has higher CHFs at high $L/s$ ratios (small $s$) as compared to the short orientation. This is probably due to the longer length of the open sides for the tall orientation as compared to the short orientation. This allows more liquid to flow in through the sides, increasing the CHF.

Surprisingly, some data points are in fact lower than this worst case correlation. Although the trend of the data follows the correlation, the values predicted seem too high.

As $L/s$ approaches zero, this correlation should correspond to unconfined pool boiling correlations. Thus, it should be able to predict the CHF data for unconfined pool boiling from vertical heaters. But, this correlation overpredicted the unconfined boiling CHF for $LN_2$ by about 30%. Thus, it appears that the constant 0.16 in the correlation should be lower. The correlation

35
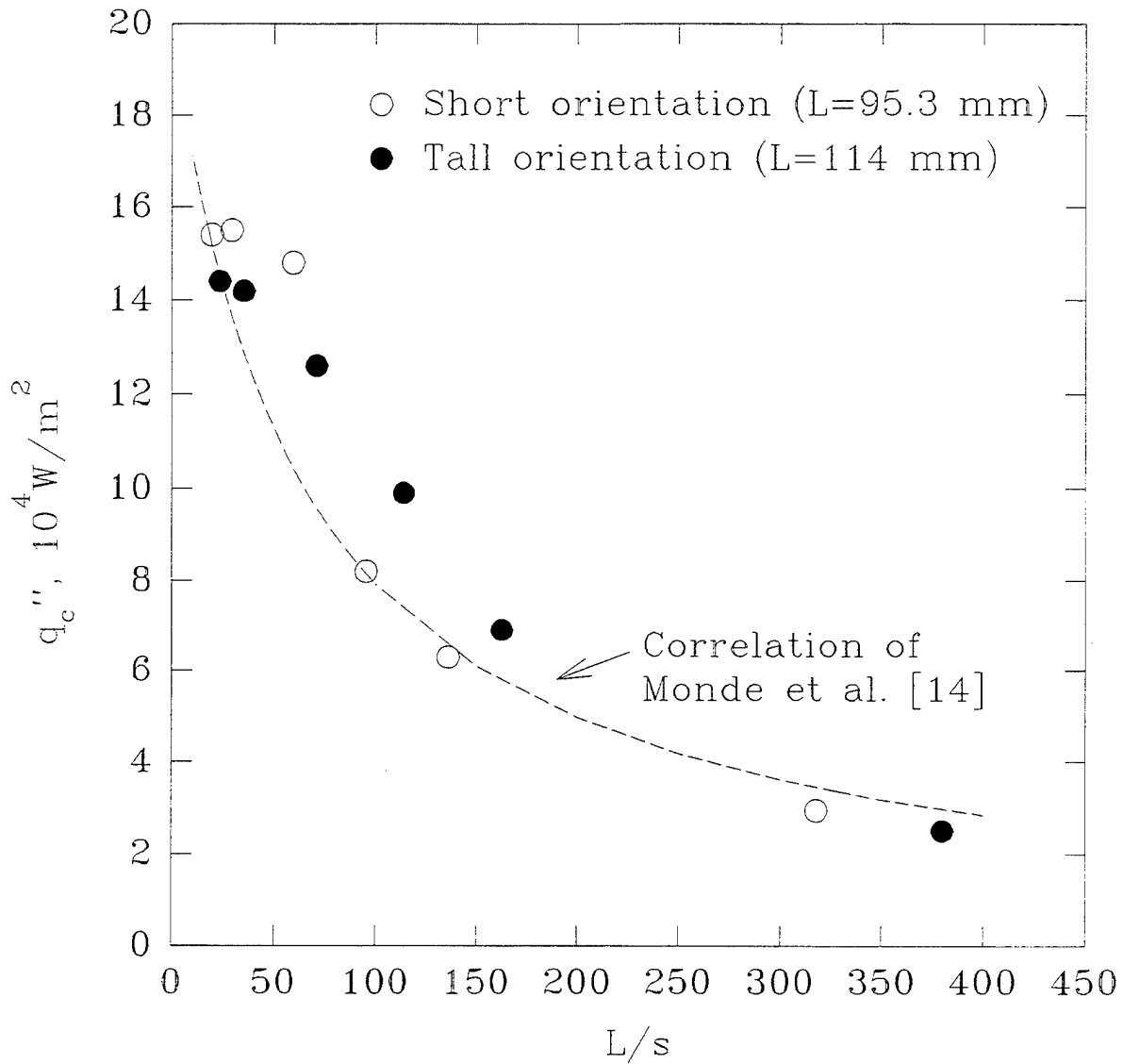
Figure 5.8 Correlation for CHF

of Lienhard and Dhir [42] which has this constant equal to 0.12 correctly predicted the CHF for unconfined pool boiling in the present study. Hence, a more conservative equation for CHF from a confined vertical array in $LN_2$ should have the constant equal to 0.12.

Finally, the results from the study may be summarised as follows:

(1) The heat transfer coefficient at lower heat fluxes generally increased as the confining plate was moved closer than 3.2 mm. The CHFs on the other hand decreased rapidly below a spacing of 1.6 mm. The increased heat transfer coefficient is due to the deformation of the bubbles which permits evaporation across a thin liquid film.

36

(2) For spacings of 0.3 mm and 0.7 mm, the CHFs from heaters closer to the bottom and side edges of the confining space were higher than the top and the middle heater in the middle column. The bottom heaters had substantially higher CHFs (up to 50% higher at $s = 0.3$ mm) as compared to heaters in the top row. The heaters in the side columns had up to 15% higher CHFs compared to the middle column.

(3) At spacings of 0.7, 1.0, 1.6, and 3.2 mm, the heat transfer coefficients from each heater operating in the array were higher as compared to those heaters operating individually. This was attributed to the thermosyphon effect. This effect is prominent at low heat fluxes. This effect diminishes below a spacing of 1.6 mm and was negligible for the smallest spacing (0.3 mm).

(4) The CHFs for the array were comparable to those for heaters operating alone. At spacings larger than 1.6 mm, the CHF in the array usually occurred at one of the lower heaters. At lower spacings, the vapor fraction at the top heaters became a factor and the CHF always occurred at the top heater in the middle column.

(5) Monde et al.'s [41] general correlation for CHF from heaters in narrow vertical channels correlated the data quite well for the array if the vertical length of the array was substituted in place of the heater length.

# 6. FLOW BOILING OF LIQUID NITROGEN FROM DISCRETE HEAT SOURCES

## 6.1 Introduction

The main focus of this research is the quantification and visualization of various geometrical effects on cryogenic boiling from discrete heat sources in a rectangular channel. Flow boiling can be broadly divided into two categories: boiling in continuously heated tubes or channels, and boiling from small discrete heat sources in a channel. In the former case, the vapor generation is a very important factor in the boiling heat transfer as channel length increases. In the boiling from discrete heaters simulating electronic chips (as in this study), the volume of vapor leaving the heated surface is generally smaller than bulk liquid flow. Therefore, the effect of vapor generation is less important. Most of the past research in flow boiling has been focussed on long continuous heated tubes. The research into the flow boiling from discrete sources in rectangular channels has received attention only recently with increasing potential for applications in electronic cooling.

This study focuses on the quantification of the critical heat flux (CHF) as well as the heat transfer coefficient of flow boiling of liquid nitrogen. The important factors that affect the CHF and heat transfer coefficient data are as follows:

a.  Flow channel geometry

The most critical parameter here is the channel height. The variation of channel height changes the flow field inside the flow channel, which will affect the CHF phenomena. Moreover, when the channel height is comparable with the dimension of vapor blanket, the vapor escape and the liquid supply routes may be blocked, leading to unexpected heat transfer and CHF results. As a matter of fact, a new theory about such situations of CHF called "thermal drag theory" has been proposed by some researchers recently [43].

b.  Surface roughness

When a surface is heated, boiling occurs from discrete sites on the surface called nucleation sites. At higher heat fluxes, the number of these sites increases. This regime is called the nucleate boiling regime and is the regime of interest because it is the most effective. Surface roughness is a key factor affecting the number of active nucleation sites and the number of active nucleation sites directly influence the heat transfer characteristics.

38

c. Heated surface dimension and spacing

In an electronic circuit board, the size and spacing of different chips vary quite a lot. How the dimensional arrangement affects the boiling heat transfer phenomena is also of great interest.

d. Heated surface protruding, recessed, or flush

According to previous research, CHF is greatly affected by these parameters, sometimes as large as 15% while the chips are only several micrometers protruding or recessed [44].

## 6.2 Design Objectives

In this study of flow boiling, it is critical to design an experimental setup that allows direct visualization to the boiling phenomena. There are several models concerning the flow boiling CHF mechanism. The most interesting one among them is proposed by Haramura and Katto [30]. They speculate that there exists a liquid macrolayer next to the heated surface, beneath the vapor bubble (shown in Figure 6.1). The thickness of this macrolayer plays the most critical role in the model. However, there is very limited evidence on the existence of this macrolayer and very little data on any measurements of its thickness. Thus, some assumptions have to be made in its estimation. This leads to inevitable deviation. The other recent model for CHF in flow boiling is due to Galloway and Mudawar [45] who observed a wavy liquid-vapor interface hovering above the heater. However, the photographic evidence supporting their model is not conclusive. Therefore, in flow boiling research at the present stage, careful visualization of the phenomena near CHF becomes crucial.

In addition to the ability of flow visualization, the experimental design should also be capable of varying the various parameters described in Section 6.1. The experimental apparatus was designed with all these factors in consideration.

## 6.3 Experimental Design

An experiment setup has been designed and manufactured based on the research focus. To allow visual access to the boiling phenomena, the setup is made of polycarbonate (a form of Plexiglass). Polycarbonate has some good thermal properties like low thermal contraction rate compared with other Plexiglasses. It also has high heat resistance, high impact strength and
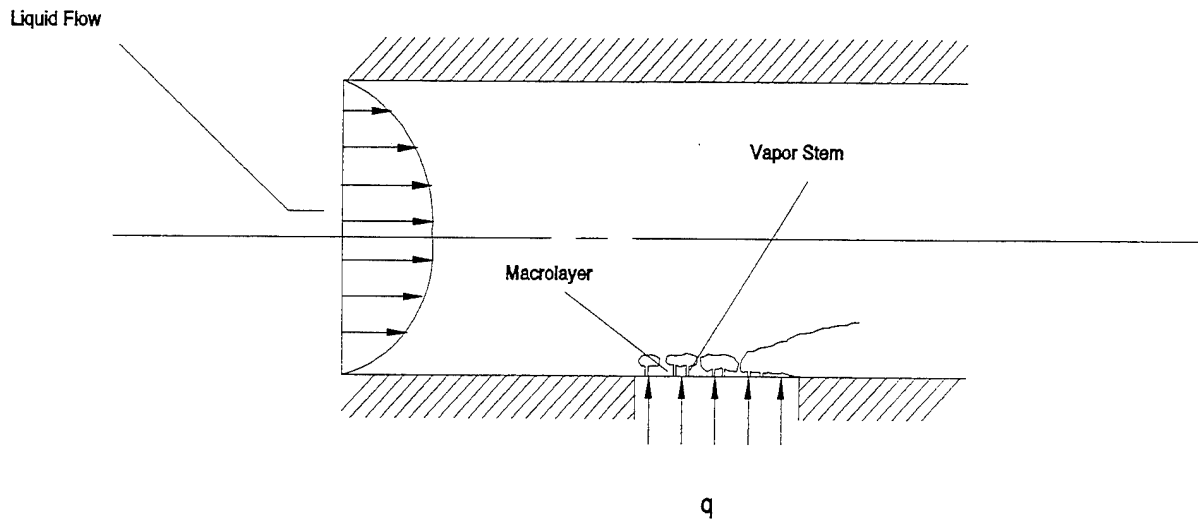
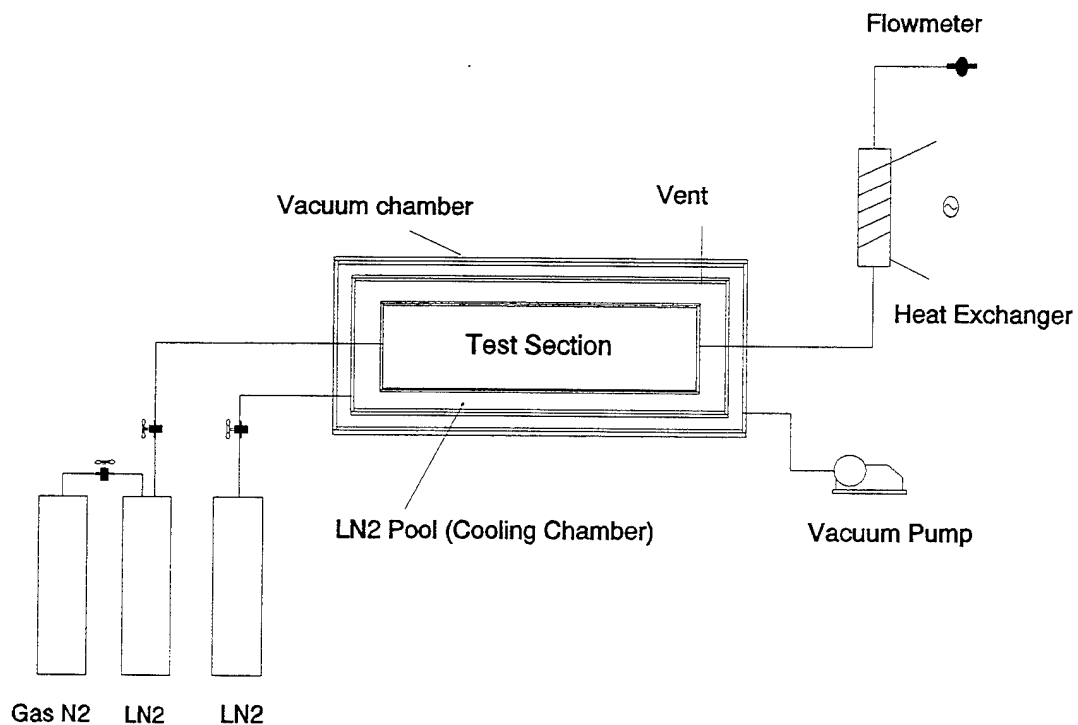Figure 6.1 Macrolayer Model for CHF



Figure 6.2  Schematic Diagram of the Experimental Setup

superb machinability. The whole setup consists of three parts as shown in Figure 6.2. The test section has three heaters (22 x 22 mm) with embedded thermocouples on the bottom of the flow

channel (see Figure 6.3). The bottom piece of the test section is exchangeable allowing various combinations of heater dimensions and spacings. The relative position of the heaters with respect to the flow channel floor can also be adjusted in order to make the heaters protruding, flush and recessed from the flow channel. The design also lets researchers adjust the channel height freely. Outside the test section is a cooling chamber. This chamber is filled with liquid nitrogen when the experiment is going on. Its function is to prevent bubble generation because of the heat conduction from the setup joints. It also serves to eliminate the heat leak from the ambient in form of radiation or conduction/convection. The section further outside is the vacuum chamber. During the experiment, vacuum is maintained in the outermost chamber to prevent water vapor in the air from forming frost outside the whole experimental setup. The vacuum also provides a good thermal insulation for the inner chambers. The liquid nitrogen pressure and the flow velocity are controlled by the pressure regulator installed before the test section. The mass flow rate of liquid nitrogen is measured after the heat exchanger by evaporating the liquid and measuring the gas flow.

During the experiments, data will be collected from the thermocouples through a Fluke data acquisition system linked to a personal computer. The power input to the various heaters will be determined by measuring the voltage and the current across the terminals. The simultaneous measurements of the heat flux (calculated from power input) and the surface temperature will allow the determination of the heat transfer characteristics.
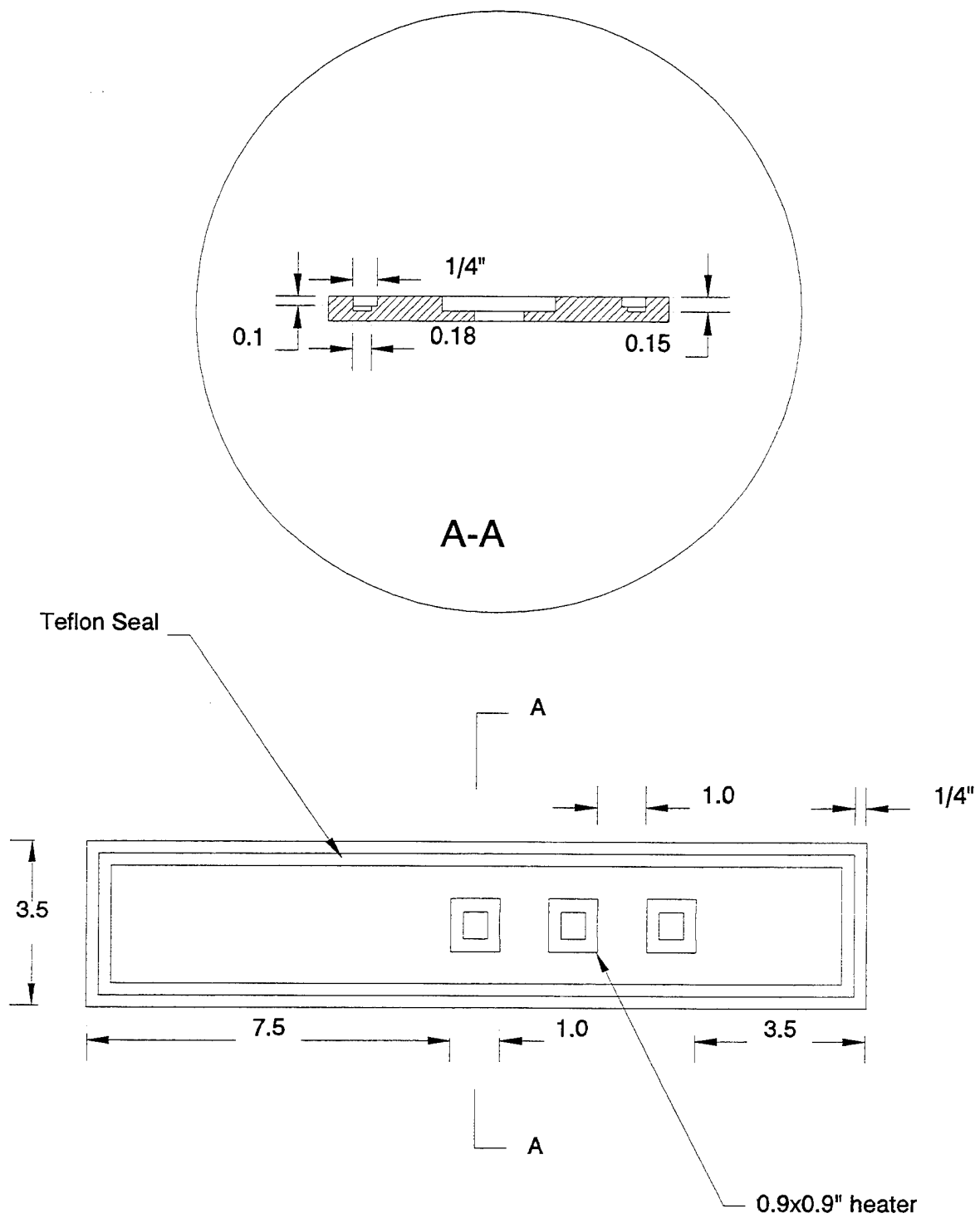
Figure 6.3  Lower Surface of the Channel

42

# 7. CONCLUSIONS AND FUTURE PLANS

The spray cooling charateristics of liquid nitrogen have been reported in previous reports. This report presented a new critical heat flux model for the spray cooling process. The resulting correlation from the model was very successful in correlating a wide array of data from various sources. This correlation is based on the macrolayer dry-out model. The main parameter which influences the magnitude of the CHF is the rate of area wetted by the spray. This parameter can be increased by having finer spray droplets for the same liquid flow rate (by employing a smaller orifice nozzle). Thus, it is possible to obtain very effective heat transfer at very low liquid flow rates. The general correlation integrates the two forms of spray cooling (air atomized and pressure atomized spray) for the first time. The effects of some important parameters (subcooling, spray uniformity, etc.) have been ignored in this correlation due to the lack of some pertinent data. Future efforts in obtaining these data should result in a refinement of this correlation. At the present time the correlation is valid for saturated liquids sprayed onto smooth surfaces.

The pool boiling characteristics of liquid nitrogen from a vertical heater array in a narrow space were studied experimentally. It was found that the CHF decreases very rapidly when the spacing in front of the heaters was reduced below 1.6 mm. At a spacing of 0.3 mm, the CHF was almost a fifth of the normal CHF. The presence of other heaters in the array did not seem to influence the heat transfer charateristics substantially at narrow spacings. The location of the heaters had a significant effect on the heat transfer charateristics. At narrow spacings, the heaters close to the lower and side edges had higher CHFs. Monde's correlation [41] for CHF from heaters in narrow channels was successful in predicting the trend of the data if the array length was used in place of the heater length. This correlation, with some minor adjustment can serve as a design correlation for a vertical array in confined space.

The flow boiling of liquid nitrogen from discrete heat sources will be studied with a focus on the effects of geometrical parameters on the CHF and the heat transfer characteristics. The design and fabrication of the experimental setup is complete and the experiments are in progress.

43

# 8. REFERENCES

1   Chow, L. C., Sehmbey, M. S., Pais, M. R., Lu, W. F., and Hahn, O. J. "Fundamental Studies in Hydrogen Blow-down and Cryogenic Cooling," Wright Laboratory Technical Report No. WL-TR-93-2081, August 1992.

2   Chow, L. C., Sehmbey, M. S., Lu, W. F., Pais, M. R., and Hahn, O. J. "Fundamental Studies in Blow-down and Cryogenic Cooling," Wright Laboratory Interim Report No. WL-TR-93-2128, September 1993.

3   Chow, L. C., Sehmbey, M. S., Hahn, O. J., and Chui, C. J., "Fundamental Studies in Cryogenic Cooling of Power Electronics," Wright Laboratory Interim Report No. WL-TR-94-2100, September 1994.

4   Nisenhoff, M., "Superconducting Electronics: Current Status and Future Prospects," *Cryogenics*, Vol. 28, No. 1, pp. 47-56, 1988.

5   Van Duzer, T., "Superconductor-Semiconductor Hybrid Devices, Circuits and Systems," *Cryogenics*, Vol. 28, No. 8, pp. 527-531, 1988.

6   Tucker, J. R., "Quantum Limited Detection in Tunnel Junction Mixers," *IEEE Journal of Quantum Electronics*, Vol. QE-15, pp. 1234-1258, 1979.

7   McGrath, W. R., Raisanen, A. V., Richards, P. L., Harris, R. E., and Lloyd, F. L., "Accurate Noise Measurements of Superconducting Quasiparticle Array Mixers," *IEEE Trans. on Magnetics*, Vol. MAG-21, pp. 212-221, 1985.

8   Fox R. M., and Jaeger R. C., "MOSFET Behavior and Circuit Considerations for Analog Applications at 77 K," *IEEE Trans. on Electron Devices,* Special Issue on Low Temperature Semiconductor Electronics, Vol. ED-34, No. 1, pp. 114-123, 1987.

9   Mueller, O., "Cryogenic Power Conversion: Combining HT Superconductors and Semiconductors," AIP Conference proceedings 251, pp. 746-759, 1991.

10  Touloukian, Y. S., Powell, R. W., Ho, C. Y. and Clemens, P. G., *Thermophysical Properties of Matter The TPRC Data Series*, Vol. 1 & 2, IFI/Plenum, NY, 1970.

11  O'Conner, L., "High-Temperature Superconducting Motors," *Mechanical Engineering*, Vol. 116, No. 4, p. 32, 1994.

12  O'Conner, L., "Building Natural Gas Locomotives," *Mechanical Engineering*, Vol. 116, No. 4, pp. 82-84, 1994.

13  Lavine, A. S., and Bai, C., "An Analysis of Heat Transfer in Josephson Junction Devices," *J. of Heat Transfer*, Vol. 113, pp. 535-543, 1991.

14  Zuber, N., "On the Stability of Boiling Heat Transfer," *J of Heat Transfer*, Vol. 80, pp. 711-720, 1958.

15  Deb, S. and Yao, S. C., "Heat Transfer Analysis of Impacting Dilute Spray on Surfaces Beyond the Leidenfrost Temperature," ASME National Heat Transfer Conf., Pittsburgh, PA, paper # 87-HT-1, 1987.

16  Awonorin, S. O., "Film Boiling Characteristics of Liquid Nitrogen Sprays on a Heated Plate," *International Journal of Heat and Mass Transfer*, Vol. 32, No. 10, pp. 1853-1864, 1989.

17  Bonacina, C., Del Giudice, S. and Comini, G., "Dropwise Evaporation," *Journal of Heat Transfer*, Vol. 101, pp. 441-446, 1979.

18  Chang, M. J., Tilford, T., Pais, M. R., Morgan, M. and Chow, L. C., "Spray Cooling of Tuna-Fish-Can Size High Performance Electronic Multi-Chip Modules," 29th ASME/AIChE

National Heat Transfer Conf., Atlanta, GA, ASME Paper 93-HT-19, 1993.

19  Pais, M. R., Chang, M. J., Morgan, M. and Chow, L. C., "Spray Cooling of High Power Laser Diodes," SAE Aerospace Conf. & Expo., Dayton, OH, SAE Paper 941183, 1994.

20  Toda, S., "A Study of Mist Cooling. 1st Report: Investigation of Mist Cooling," *Heat Transfer Japanese Research*, Vol. 1, No. 3, pp. 39-50, 1972.

21  Monde, M., "Critical Heat Flux in the Saturated Forced Convection Boiling on a Heated Disk with Impinging Droplets," *Heat Transfer - Japanese Research*, Vol. 8, pp. 54-64, 1979.

22  Choi, K. J., and Yao, S. C., "Mechanism of Film Boiling Heat Transfer of Normally Impacting Spray," *International Journal of Heat and Mass Transfer*, Vol. 30, No. 2, pp. 311-318, 1987.

23  Pais, M. R., Chow, L. C., and Mahefkey, E. T., "Surface Roughness and its Effects on the Heat Transfer Mechanism in Spray Cooling," *Journal of Heat Transfer*, Vol. 114, pp. 211-219, 1992.

24  Sehmbey, M. S., Chow, L. C., Hahn, O. J. and Pais, M. R., "Effect of Spray Characteristics on Spray Cooling with Liquid Nitrogen," *Journal of Thermophysics and Heat Transfer*, Vol. 9, No. 4, pp. 757-765, 1995.

25  Yang, J., "Spray Cooling with an Air Atomizing Nozzle," Ph.D. Dissertation, University of Kentucky, Lexington, KY, 1993.

26  Cho, C. S. K. and Wu, K., "Comparison of Burnout Characteristics of Jet Impingement Cooling and Spray Cooling," National Heat Transfer Conf., Houston, HTD-Vol. 96, pp. 561-567, 1988.

27  Tilton, D. E., "Spray Cooling," Ph.D dissertation, Univ. of Kentucky, Lexington, KY, 1989.

28  Kopchikov, I. A., Voronin, G. I., Kolach, T. A., Labuntsov, D. A., and Lebedev, P. D., "Liquid Boiling in a Thin Film," *International Journal of Heat and Mass Transfer*, Vol. 12, pp. 791-796, 1969.

29  Grigor'ev, V. A., and Dudkevich, A. S., "Boiling Cryogenic Liquid in a Thin Film," *Teploenergetica*, Vol. 17, No. 12, pp. 54-57, 1970.

30  Haramura, Y., and Katto, Y., "A New Hydrodynamic Model of Critical Heat Flux Applicable Widely to Both Pool and Forced Convection Boiling on Submerged Bodies in Saturated Liquids," *International Journal of Heat and Mass Transfer*, Vol. 26, No. 2, 1983, pp. 389-399, 1983.

31  Kumada, T., and Sakashita, H., "Proposed Model for Kutateladze Correlation and New Correlation of CHF," *Pool and External Flow Boiling*, edited by V. K. Dhir and A. E. Bergles, ASME press, NY, pp. 177-183, 1992.

32  Sehmbey, M. S., Pais, M. R., and Chow, L. C., "Effect of Surface Material Properties and Surface Characteristics in Evaporative Spray Cooling," *Journal of Thermophysics and Heat Transfer*, Vol. 6, No. 3, pp. 505-512, 1992.

33  Lefebvre, A. H., *Atomization and Sprays*, Ch 6., Hemisphere, NY, 1989.

34  Mirza, S., "The Behavior of Liquid Nitrogen from Aluminum Surfaces," *Int. Comm. Heat Mass Transfer*, Vol. 17, No. 1, pp. 9-18, 1990.

35  Tuzla, K., Çökmez-Tuzla, A.F., Crowley, A.J. and Chen, J.C., "Cooling of Electronic Chips in Liquid Nitrogen," Proceedings of the Ninth Int. Heat Transfer Conf., Jerusalem, Israel, Heat Transfer, Vol. 2, Editor: G. Hetsroni, pp. 301-306, 1990.

36 Mudawar, I. and Anderson, T.M., "High Flux Electronic Cooling by Means of Pool Boiling - Part I: Parametric Investigation of the Effects of Coolant Variation, Pressurization, Subcooling, and Surface Augmentation." 1989 National Heat Transfer Conf., Heat Transfer in Electronics, HTD-Vol. 111, pp. 25-34, 1989.

37 Chui, C. J., Sehmbey, M. S., Chow, L. C., and Hahn, O. J., "Pool Boiling Heat Transfer from Vertical Heater Array in Liquid Nitrogen," *J. Thermophysics and Heat Transfer*, Vol. 9, No. 2, pp. 308-313, 1995.

38 Fujita, Y., Ohta, H., Uchida, S., and NIshikawa, K., "Nucleate Boiling Heat Transfer and Critical Heat Flux in Narrow Space between Rectangular Surfaces," *Int. J. Heat Mass Transfer*, Vol. 31, No. 2, pp. 229-239, 1988.

39 You, S.M., Simon, T.W., and Bar-Cohen, A., "Pool Boiling Heat Transfer with an Array of Flush-Mounted, Square Heaters," Topics in Heat Transfer, HTD-Vol. 206-2, ASME, pp. 63-72, 1992.

40 Polentini, M.S., Ramadhyani, S., and Incropera, F.P., "Two-Phase Thermosyphon Cooling of an Array of Discrete Heat Sources in a Rectangular Cavity," Advances in Electronic Packaging, EEP-Vol. 4-2, ASME, pp. 899-908, 1993.

41 Monde, M., Kasuda, H., and Uehara, H., "Critical Heat Flux During Natural Convection Boiling in Vertical Rectangular Channels Submerged in Saturated Liquid," *J. Heat Transfer*, Vol. 104, pp. 300-303, 1982.

42 Lienhard, J. H., and Dhir, V. K., "Hydrodynamic Prediction of Pool-Boiling Heat Fluxes from Finite Bodies," *J. Heat Transfer*, Vol. 95, pp. 152-158, 1973.

43 Guo, Z., and Bu, W., "Thermal Drag in Forced Duct Flows," *International J. of Heat and Mass Transfer*, Vol. 34, No. 1, pp. 229-235, 1991.

44  Leland, J. E., "The Effects of Channel Curvature and Protrusion Height on Nucleate Boiling and the Critical Heat Flux of a Simulated Electronic Chip," Air Force Wright Laboratory Technical Report, WL-TR-94-2051, May 1994.

45  Galloway, J. E., and Mudawar, I., "CHF Mechanism in Flow Boiling from a Short Heated Wall, Part I and II," *International J. Heat and Mass Transfer*, Vol. 36, No. 10, pp. 2511-2540, 1993.